# Delivery of Macromolecule Therapeutics via Jetting in the Gastrointestinal Tract

by

Graham Arrick

Submitted to the
Department of Mechanical Engineering
in Partial Fulfillment of the Requirements for the Degree of

Master of Science in Mechanical Engineering

at the

Massachusetts Institute of Technology

May 2020



Signature of Author: _____

Department of Mechanical Engineering
May 15th, 2020

Certified by: _____

Carlo Giovanni Traverso
Assistant Professor of Mechanical Engineering
Thesis Supervisor

Accepted by: _____

Nicolas Hadjiconstantinou
Professor of Mechanical Engineering
Chairman, Department Committee on Graduate Theses

# Delivery of Macromolecule Therapeutics via Jetting in the Gastrointestinal Tract

by

Graham Arrick

Submitted to the Department of Mechanical Engineering
on May 15th, 2019, in Partial Fulfillment of the
Requirements for the Degree of

Master of Science in Mechanical Engineering

## Abstract

Biologics are a class of therapeutic substances composed of large and complex "macromolecules." Examples include vaccines, insulin, monoclonal antibodies, and allergens. However, a practical limitation of these molecules is that they are easily degraded by digestive processes and, as a result, are not generally considered effective for oral dosing. Therefore, these life-saving drugs are typically delivered via intravenous, intramuscular or subcutaneous injection. Oral administration, however, yields some of the highest patient adoption and adherence rates, and is often critical in determining a drug's efficacy. Herein lies the goal of this research: to make it possible to successfully deliver a broad set of biologics by mouth. To that end, needleless delivery, or *jetting*, has been identified as a promising approach. This work describes mechanistic modeling of jets, an empirical evaluation of jet interaction with gastrointestinal tissues, a millimeter-scale jetting device capable of autonomous drug delivery, and in-vivo studies in which the tested devices elicit substantial drops in blood glucose levels via the delivery of insulin across the gastric mucosa.

Thesis Supervisor: Carlo Giovanni Traverso
Title: Assistant Professor of Mechanical Engineering

# Acknowledgements

First and foremost, the author would like to thank Miss Yi “Louise” Lu of the University of Toronto for her consistent dedication to our work as well as her overwhelming positivity and general kindness. The execution of much of our experiments, as well as the formulation of this document would not have been possible without her.

Secondly, the author would like to thank Declan Gwynne and Jake Wainer for being excellent engineers, co-workers and, above all, friends. Their ongoing support with mechanical design analysis and testing, as well as their creativity has been a crucial part of this effort.

The author would also like to thank Torben Sebastian Last of the Kungliga Tekniska Högskolan, who is an extremely disciplined scientist and a great friend. His ideas, consultation, analysis and moral support (as well as his home cooking), were all critical in the success of this thesis.

Next, the author would like to extend a word of appreciation to Alex Abramson, Jason Li, Siheng “Sean” You, and Param Karandikar—researchers in our group whose wisdom was enlightening in the face of uncertainty.

The author would also like to extend gratitude to Novo Nordisk, not only for providing funding for this project, but for providing access to brilliant scientists and engineers. The author is particularly grateful for the ideas contributed by Drago Sticker, Aghiad Ghazal, Morten Frederiksen, Brian Jensen and Dan Sørensen.

A great deal of thanks is owed to our wonderful veterinary technicians (present and former), including Joy Collins, Siddartha Tamang, Keiko Ishida and Cody Cleveland, whose expertise and flexibility made the documented in vivo work possible. The author also owes much thanks to the Autotiv machine shop for its ability to quickly produce high quality millimeter-scale parts.

Finally, the author would like to thank Professor Carlo Giovanni “Gio” Traverso of the Massachusetts Institute of Technology, for his constant optimism and his uncanny ability to think outside of the box. Gio’s unwavering support of the author’s efforts, as well as his keen guidance on project management, were essential in realizing ingestible jetting. Gio’s dedication to innovation is only rivaled by his dedication to creating a caring and inclusive community.

# Table of Contents

# Table of Figures

# 1 Introduction

Within the fields of pharmacology and molecular biology there exist two broad classes of molecules: small molecules and macromolecules. Small molecules readily diffuse through cell membranes, and can be absorbed into the bloodstream through the digestive process. Macromolecules weigh more than 900 Daltons, and do not readily undergo trans-cellular diffusion [1][2][3]. Macromolecules are synthesized through biological processes—thus, they are often referred to as "biologics."

Historically, small molecules have been used in pharmacology more widely than biologics. This is due to their comparatively low cost and their simplicity of administration [4]. As evidence of this: small molecules have accounted for more than 70% new of drugs available on the market since 1996 [5]. That said, sales of biologics have come to play a much more significant role in the market in recent years. According to an annual report on pharmaceuticals, in 2016 "biologics accounted for six of the top-eight drugs, in terms of revenue... [Humira] led the way, with a total of $18.4 billion sales". Also, according to the same source, "the global biologics market is expected to register a [cumulative growth] of about 10.5% during the 2018-2023 forecast period" [6].

These trends can be attributed to advances in pharmacologic technology that have enabled the synthesis of more complex molecules [4]. Furthermore, there has been a significant increase in chronic diseases that necessitate biologic treatments. For example, in the United States, the number of patients carrying a diagnosis of Diabetes Mellitus (diabetes) rose from approximately 6% of the population (16.9 million) in the year 2000, to 9% of the population (29.7 million) in 2018 [7]. The discovery of new macromolecule treatments for other diseases such as plaque psoriasis, Crohn's disease and cancer has contributed to the growth of the biologics market as well.

Despite their clear value, a key limitation of biologics is that they cannot be administered orally, as digestive acids and enzymes cause these molecules to degrade before they are absorbed into the bloodstream [1]. To rephrase: biologics have low bioavailability when swallowed, and as a result, they are widely administered through other methods such as subcutaneous injection, intravenous infusion or wearable pumps. These methods of administration are considered to be more invasive than the oral route, and are widely believed to lead to problems with patient adherence.

## 1.1 The Problem: Non-adherence to Biologic Dosing Regimens

Adherence is defined by the World Health Organization as "the extent to which a person's behavior—taking medication, following a diet, [or] executing lifestyle changes—corresponds with agreed recommendations from a health care provider" [8]. Failure to adhere is called "non-adherence." Non-adherence exists no matter what disease a patient has, no matter what type of treatment is recommended by their healthcare provider, and no matter what level of accessibility the patient has to healthcare resources. Lapses in patient adherence result in a reduced quality of life, increases in morbidity and mortality rates, and wasted health care resources [9]; in the United States, up to 10% of hospitalizations are the result of poor medication adherence [8].

As noted previously, biologics' low bioavailability necessitates the use of invasive routes of administration. This means that for biologics, drug routine adherence is *especially* low. Up to 45% of patients diagnosed with Type 2 diabetes do not adhere to their prescribed treatments (the main treatment being self-administration of insulin) [9]. Patients with diabetes who do not receive proper therapeutic treatment can experience prolonged hyperglycemia resulting in dehydration, fatigue, weight loss, nerve damage, further reductions in pancreatic function, kidney failure, and even coma or death.

A study on adherence to subcutaneous injection of insulin revealed that patients attribute their failure to adhere to a number of shortcomings of biologics. Among these are perceived complexity associated with preparing injections, pain or irritation from injections, and fear of needles [10][11]. Additionally, the high price of insulin as well as challenges associated with insurance coverage further reduce adherence [12].

In summary, despite the fact that many life-saving biologic treatments have been developed, the healthcare system still experiences a tremendous burden due to these medications'

amplification of adherence issues. Thus, there are broad-reaching efforts to improve biologics by streamlining their administration. For example, patients are known to prefer auto-injectors over syringes and, as a result, numerous healthcare providers recommend them as a means for administration [13][14]. Moreover, advances in "smart" technology have simplified the use of continuous insulin pumps.

The work detailed in this thesis seeks to address the problem of patient non-adherence to macromolecule treatments by implementing an ingestible device for the oral delivery of a broad range of biologics. The use of such a device would be identical to that of a typical small-molecule therapeutic tablet. Rather than passive chemical absorption however, the device incorporates an onboard actuation mechanism and means for self-triggering. The thesis identifies needleless injection, or *jetting*, as a simple and effective means for penetrating the gastrointestinal (GI) mucosa, and delivering liquid depots for systemic uptake. Topics covered include the fundamental mechanics of jetting, an empirical evaluation of jetting in multiple types of tissue, design of an autonomous, cm-scale device, and a demonstration of concept feasibility through in vivo testing in a large-animal model. The data presented in this thesis suggests that jetting represents a promising path for the future of oral delivery of macromolecules, and could also be applicable to other GI-based procedures such as endoscopic injections.

## 1.2 History of Jetting

The earliest known needleless injector was described in Gelante and Béclard's report of an instrument for performing aquapuncture in an 1866 issue of the *Gazette Médical de Paris* [15][16]. Note that this was only 13 years after the introduction of the hypodermic needle [17]. Subsequent reports of the aquapuncture device could not be located.

Decades later, in 1929, a mechanical engineer from New York named Arnold K. Sutermeister, began developing a needleless injection mechanism. Sutermeister had been inspired by his past observations of inadvertent penetration by pressurized oil into the flesh of engine workmen. Following promising experimental results, Sutermeister shared his work with doctors at the New York Presbiterian Hospital and Columbia University, who later disclosed the concept to the Cambridge Instrument Company [16].

The earliest known patent for a needleless delivery mechanism was granted to Marshall L. Lockhart of Detroit, in 1943 [18]. Lockhart learned of Stutermeister's device during his time

working at the Cambridge Instrument Company, and independently developed a much-improved version [16][18]. Lockhart was later employed by the Gelatin Products Corporation and by Becton, Dickinson & Co. Both companies eventually claimed intellectual property rights over Lockhart's device [16].

Since Stutermeister and Lockhart's time, over 2000 patents relating to needleless devices have been granted to various companies and inventors [19]. **Table 1.1** summarizes the intellectual property space for needleless devices since 1940.

**Table 1.1:** Intellectual property space for needleless delivery since 1940 [19]

| Time-period | Num. of Needleless patents during time-period | Company with most patents granted | Company's share of time-period patents |
|---|---|---|---|
| 1940-1960 | 98 | Becton, Dickinson & Co | 27% |
| 1960-1980 | 97 | Scherer - Gelatin Products Corp. | 12% |
| 1980-2000 | 574 | Bioject Med. Tech. | 7% |
| 2000-2020 | 1361 | Antares Pharmaceuticals | 8% |

Most jetting systems are designed to have a high initial "peak" pressure, which serves to quickly form a hole in the skin. This hole allows for the injection of the remaining volume at a lower "delivery" pressure. Peak and delivery pressures for a sample set of historical jetting devices have been tabulated in **Table 1.2**, along with their respective nozzle orifice diameter. These orifices generally have diameters smaller than the outer diameter of a 30 Gauge hypodermic needle [20].

**Table 1.2:** Summary of historical needleless devices with estimated peak and delivery pressures [19][21]

| Year | Patent number | Inventor | Company | Orifice diameter (µm) | Peak pressure (Bar) | Delivery pressure (Bar) |
|---|---|---|---|---|---|---|
| 1943 | US2322245 | Lockhart | - | 100 | 710 | - |
| 1956 | US2754818 | Scherer | Gelatin Prod. | 50-250 | 710 | 140 |
| 1995 | US5399163 | Peterson et al. | Bioject | 80-130 | 280-310 | 80-140 |
| 1997 | US5599302A | Lilley et al. | Antares | 165 | >140 | 100-140 |
| 2011 | US20110288521A1 | Bingham | PharmaJet | 180 | 225 | - |
| 2017 | US20170143906A1 | Coats & Dyer | Portal | 50-350 | >110 | 70-110 |

Despite its regular use, however, this technology has never been applied to achieve submucosal delivery from an autonomous pill in a clinical setting. The closest embodiment was reported by Aran et al. [22] but, as will be discussed shortly, this device is neither ingestible, nor does it develop pressures that are sufficient to create submucosal depots in GI tissue. Additionally, Baywind Bioventures has reported an ingestible jetting device, but has provided little data on performance or tissue penetration characteristics [23].

## 1.3 Prior Art in the Oral Delivery of Biologics

To date, dozens of solutions have been proposed for the oral delivery of biologics. Methods range from direct penetration of the mucosa by solid micro needles to excipient-based modification of local enzymatic activity in the GI tract. Unfortunately, few solutions have produced 'double-digit' bioavailability (i.e greater than 10%), which would be an essential step for practical use [11][24]. This section presents a brief review of previous solutions for the delivery of biologics as a means for providing further context for the proposed work in this thesis.

### 1.3.1 Jetting

It is important to acknowledge that jetting has been employed in the past for the oral delivery of macromolecules. The first example was reported by Aran et al. with their device called "MucoJet." This device is held in the mouth against the mucosa, while the hydration of an internal acid-base matrix results in pressurization of the device and subsequent expulsion of the jet [22]. MucoJet, however, is only reported to provide superficial penetration of the mucus layer (not the epithelium). Though this may be sufficient for mucosal immunization purposes, no data has been provided for submucosal delivery of other important biologics such as insulin.

Aside from MucoJet, at least two other ingestible jetting devices have been disclosed in patent databases. These include WO2020041774 (Baywind Bioventures) and WO2018049133 (Progenity/StarFish Medical) [25][26]. Though high bioavailability is promised by these devices, no ex vivo or in vivo data could be located.

### 1.3.2 Solid Micro- and Mili-needles

Abramson et. Al demonstrated a device capable of delivering macromolecules with high bioavailability via the oral route. This device employs a spring-actuated millimeter-scale needle (mili-needle) which is passively localized to the stomach mucosa via self-orientation. Delivery of

the mili-needle is triggered via dissolution of a structural carbohydrate member. The needle in this device was reported to create a penetration wound (approximately 1mm in diameter) at the site of injection. However, this side-effect was not proven to cause health complications in in vivo swine studies [27].

The luminal unfolding microneedle injector (LUMI) is another example of a device platform that seeks to orally deliver macromolecule drugs by use of dissolvable needles. This system is designed to deploy and expand in the small intestine. It has three biodegradable arms, each bearing a patch of 1-mm-long, dissolvable, drug-loaded microneedles. The device is contained in a capsule comparable in size to a 000 pill. This capsule is sealed by an enteric polymer that dissolves upon entry into the small intestine, allowing for release of the device. The LUMI demonstrated bioavailability larger than 10% over a 4-hour sampling period [28].

Rani Therapeutics, a company focused on devices for oral delivery of therapeutics, has also proposed a system for delivering solid mili-needles in the small intestine [29][30].

### 1.3.3 Liquid Injection with Hypodermic Needle

Hypodermic injection has been used to deliver biologics such as epinephrine to the GI tract (through use of an endoscope) [31]. Though no reports of an autonomous device designed to inject the mucosa with a hypodermic needle have been located, it would certainly be possible to implement such a device. This device would require a mechanism to deploy the needle, deliver the dose, and retract the needle.

### 1.3.4 Absorption Enhancers

Absorption enhancers, often referred to as permeation enhancers, are excipients that could allow macromolecules to more readily transverse barriers to systemic uptake such as the mucosal epithelium [32]. A class of an absorption enhancers that has received attention recently is Ionic Liquids. These compounds have been demonstrated to both enhance diffusion through the epithelial barrier, as well as decrease enzymatic activity at the site of deployment. The functional mechanisms for ionic liquids are not well understood, but they show promise for oral delivery of biologics [24].

Yet another recent advance in absorption enhancement of biologics was demonstrated by Buckley et al. in their study of sodium N-[8-(2-hydroxybenzoyl) aminocaprylate] (SNAC) as an excipient for oral Semaglutide. In this study, the authors demonstrated that SNAC increased the

solubility of Semaglutide as well as performing other functions to assist with absorbtion. That said, the authors report that the use of SNAC based excipients still only offers single-digit bioavailability [33].

### 1.3.5 Enzyme Inhibitors

Certain compounds have been proven to limit the impact of digestive enzymes on the degradation of orally administered biologics. Protease inhibitors for example, bind to active sites on protease enzymes, limiting their metabolizing functions. As an excipient, protease inhibitors have been shown to protect macromolecules from degradation [24].

Inhibition of enzyme activity can also be achieved by altering the local pH in the lumen as certain enzymes only function at a specific pH. For example, citric acid, used as an excipient for an oral formulation of recombinant salmon calcitonin (TBRIA), was shown to lower the local pH of the duodenum, thereby inhibiting proteases from degrading the active biologic [24]. Buckley et al. reported that SNAC had the effect of raising local stomach pH, thereby protecting Semaglutide from pepsin as well.

### 1.3.6 Nanotechnology

Nanotechnology, in the context of drug delivery, usually refers to engineered vehicles that vary in size from 10 nm to 1000 nm [34]. An example of a nano-vehicle is a solid, polymeric or metallic sphere with biologics conjugated to the surface or embedded within its constitutive matrix [34]. Nano-vehicles can also be a hollow sphere, or nano-capsule, with the active agent contained in its center. Though there is much left to be understood, these vehicles have been observed to selectively permeate different cell types depending on factors such as vehicle size and surface chemistry. They are also thought to protect macromolecules by providing a physical barrier against enzymatic interaction. Current challenges in the field of nano-vehicles include toxicity, long-term stability and pH sensitivity [35] [36].

Another example of nanotechnology for delivery of biologics is the use of exosomes. Exosomes are a type of naturally synthesized extracellular vesicle (EV). They have diameters ranging from 30 to150 nm and are theorized to be employed in intercellular signaling mechanisms. Recent research efforts have aimed to modify these EVs for containment of proteins, lipids and genetic materials for the purpose of drug delivery. Exosomes show particular promise as they are non-immunogenic by nature [37][38].

### 1.3.7 Iontophoresis

Iontophoresis is a type of transdermal drug delivery technique which could be employed for oral delivery of biologics. It is used to enhance flow of charged molecules through cellular barriers by providing a potential drop through the subject tissue [39]. Though implementation of an ingestible iontophoresis device would require significant miniaturization of contemporary driving electronic systems, recent advances in power technology could enable their implementation [40]. That said, iontophoresis has been used to enhance local delivery of macromolecules in the oral cavity [41].

## 1.4 Biologics

There are many different biologics that could be deployed by an ingestible jetting device. As such, ingestible jetting should be considered a platform technology. That said, insulin was selected as a model drug given its clinical ubiquity and the fact that insulin produces an immediate drop in blood glucose (BG) which can be directly observed during experiments without bioanalysis. This section briefly details each type of biologic that was considered for this work and which could be used in future work.

### 1.4.1 Molecules for Glycemic Control

Insulin is a peptide hormone secreted by the beta cells of the pancreatic islets. It is involved in multiple anabolic processes such as glucose uptake, and regulating carbohydrates, lipids and proteins. Insulin was discovered by Banting, Best and Macleod at the university of Toronto in 1921, and was first used for treatment of diabetes in 1922 [42]. It is a dipeptide with 51 amino acids and a molecular weight of approximately 5800 Daltons. Insulin helps convert sugars into energy which is eventually stored in muscle, fat cells and the liver. It accomplishes this through glycolysis, glycogenesis and lipogenesis. These functions, among others, lead to a reduction in blood glucose concentration [43].

Glucagon-like Peptide-1 (GLP-1) receptor agonists, which mimic GLP-1s, have also proven effective for glycemic control. GLP-1 is a naturally occurring incretin hormone which both stimulates insulin secretion and inhibits glucagon secretion [44]. It has also been shown to play a role in gastrointestinal activity such as motility and mucus secretion, and appears to have a neurological impact, causing reductions in appetite [45]. As a result of the above functions GLP-1 receptor agonists have been marketed widely for the treatment of diabetes. Examples of commercially available GLP-1 agonists include Albiglutide, Liraglutide and Semaglutide.

### 1.4.2 Vaccines

Vaccines protect against dozens of infectious diseases by helping the body's immune system to recognize and combat pathogens. They accomplish this by introducing a weakened form of the pathogen so that the immune system can safely recognize the threat and produce protective antibodies for future use. Vaccines are recommended to be given early in life when the patient is most vulnerable and many vaccines require more than one dose for long-lasting protection. Most vaccines are injected subcutaneously or intramuscularly. Though some solutions have been demonstrated, for the majority of vaccines, oral delivery remains a challenge [46].

### 1.4.3 Monoclonal Antibodies

Monoclonal antibodies (MABs) are human-synthesized antibodies generated from a single B-cell clone. MAB drugs can help the immune system in various way including: flagging cancer cells, triggering cell-membrane destruction, blocking cell growth, blocking immune system inhibitors, and by directly attacking cancer cells [47][48]. MABs are used to treat cancer, rheumatoid arthritis, multiple sclerosis, cardiovascular disease, systemic lupus erythematosus, Crohn's disease, ulcerative colitis, psoriasis, transplant rejection, and other diseases [49]. To date, MABs have been designed to be administered by subcutaneous injection or intravenous infusion. Examples include Adalimumab, Alemtuzumab and Rituximab. Of note, Adalimumab (Humira) was the number one selling drug in 2019 [50].

### 1.4.4 Therapeutic Protease Inhibitors

Protease inhibitors play an important role in multiple antiviral treatments to combat human immunodeficiency virus (HIV), as well as other diseases. Certain protease enzymes are known to promote HIV viral maturation and proliferation. Therapeutic protease inhibitors prevent this by occupying active sites on the protease enzyme. Protease inhibitors are generally considered small molecules however, significant challenges have been encountered in improving their oral bioavailability [51][52].

### 1.4.5 Hormones

Hormones are a type of signaling molecule secreted by several glands within the body. They are essential for growth, metabolism, sexual function, mood, and other bodily functions. Examples include insulin, estrogen, progesterone, prolactin, testosterone, serotonin, cortisol, and adrenaline.

Hormone therapy has been reported to treat cancer by altering the local hormonal content of cancerous cells, thereby impeding their proliferation [53]. Another common use is hormone replacement therapy, in which hormones are administered to offset bodily hormone deficits that result from disease or aging (e.g. diabetes and menopause [54]).

### 1.4.6 Allergens

Injection of allergens is a type of immunotherapy used to reduce the host's reaction to the subject allergen by regular fixed, or incrementally increasing exposure. This has been proven to reduce or even eliminate certain food allergies, allergies related to animal contact, and environmental allergies [55]. As an example, during a typical pollen hyposensitization therapeutic regimen, injection of allergen extracts can be employed multiple times per week [56].

## 1.5 Gastrointestinal Anatomy

A brief review of gastrointestinal tissue anatomy is provided including tissue thickness, cell layering, and other properties as these factors could affect jetting performance. Generally GI tissue is composed of four broad cell layers: the mucosa, which secretes mucus, and acts as the first barrier to absorption of substances such as macromolecules; the submucosa, which is rich with vasculature and carries nutrients to and from the mucosa, the muscularis, which is responsible for motility, and the serosa which functions as the outermost, protective layer for each organ. A summary of organ physical properties is provided in **Table 1.3**.

**Table 1.3:** Summary of GI organ physical properties [57][58][59][60][61][62][63][64][65][66]

| Organ | Length | Diameter | Overall Wall Thickness | Emptying Time |
|---|---|---|---|---|
| Cheek (Buccal) | N/A | N/A | ~8mm | ~30s |
| Esophagus | 25 – 33 cm | ~2cm | 2 – 5mm | 6 –15s |
| Stomach | 26 – 3 cm | 8 – 10cm (max) | 3 – 5mm | 3 – 5 hours |
| Small intestine | 2 – 6 m | 2 – 4cm | 1 – 2mm | 2 – 6 hours |
| Large intestine | ~1.5 m | 6 – 8cm | 1 – 5mm | 10 – 60 hours |
| Rectum | 10 – 15 cm | 4 cm (max) | 2 – 4mm | 10 – 72 hours |

### 1.5.1 Buccal Space

The buccal space, or oral cavity, is the first organ in the digestive process. In the cheek, a unique type of squamous epithelial cell makes up the basal mucosa, and secretes a continuous supply of mucin [67]. Other than the epithelial and mucosal cells, muscles, fat and connective tissue are all present in the cheek. Jetting in the buccal space has been demonstrated for dental applications [68] and by MucoJet [22], but could be less desirable for regular dosing due to nerves in the mouth that can detect sharp pain [69].

### 1.5.2 Esophagus

The function of the esophagus is to transfer food from the mouth to the stomach. Lymph nodes, which store lymphocytes and filter foreign bacteria and substances from lymph fluid, are present within and nearby the esophageal structure. The esophagus is 25-33 cm in length in adults, and is 1.5 to 2cm in diameter, with a wall thickness of 2 to 5mm [58][59]. Though pain receptors exist in the esophagus, they tend to transmit more generalized sensation such as pressure or distension, rather than sharp pain [58]. Jetting in the esophagus could be desirable as tissue localization would not be a challenge. However, the short transit period (as short as six seconds [61]), would make timely triggering difficult.

### 1.5.3 Stomach

The function of the stomach is to break down ingested food before it is passed into the intestine. Acidic gastric fluid (containing hydrochloric acid) and enzymes (such as pepsin) transform the food into chyme, and allow for initial uptake of nutrients [70]. The stomach consists of four regions: the cardia, fundus, body and pylorus. The cardia is where the esophagus connects to the stomach. Adjacent to and above the cardia, is the fundus, which expands and contracts according to volumetric intake [57]. Below the fundus is the largest part of the stomach, the body, which functions as the reservoir for food, chyme and liquid. The pylorus is funnel-shaped, and features a sphincter, controlling the entry of food into the duodenum and intestine. The larger exterior portion of the stomach is referred to as the Greater Curvature, and the small part, the Lesser Curvature. Food tends to sit in the lower pyloric antrum, near the stomach's base. The pH of the stomach is between 1.5 and 3.5 [70].

### 1.5.4 Small Intestine

The small intestine is the site of terminal food digestion, where nutrients are absorbed by cells of the epithelial lining [71]. The small intestine is the longest GI organ (200cm in infants to 600cm in adults [62]) and made of three parts: duodenum, jejunum and ileum. The intestinal wall is relatively thin (2-3mm [63]), which could create a risk of perforation for a jet. However, the relatively small diameter of the small intestine makes it appealing since all sides of a device would be in close proximity to the intestinal wall.

### 1.5.5 Large Intestine

The large intestine absorbs water from the remaining bolus, and then passes the waste to the rectum. The large intestine consists of five parts: the cecum, ascending colon, transverse colon, descending colon, and sigmoid colon. The large intestine has similar tissue layering and thickness to the small intestine, though it is much shorter, wider, and does not contain villi [72][64]. The large intestine is likely not a desirable location for an autonomous jetting device given the possibility of interference by a solid bolus. However, it could be possible to perform endoscopic administration of jets in the colon via the rectum.

### 1.5.6 Rectum

The rectum is the final step in digestion, where stool is formed and eventually passed out of the system. Rectal tissue is thicker than that of the small intestine owing to the presence of muscles for passage of the stool [73][65]. Like the colon, the rectum would be best suited for endoscopic administration of a jet.

# 2 Jetting Mechanics

Jetting has been in use for decades for vaccination, delivery of insulin, and other purposes. A jetting device, contains a liquid reservoir which is energized (usually) by means of a spring or compressed gas. Once the liquid is energized, it is formed into a columnar jet via a nozzle, and the jet is used to penetrate one or multiple layers of biological tissue. This chapter develops a simple mechanistic model for a spring-based jetting system, and details an experimental validation of the model using a laboratory jetting test stand and high-speed force sensor.

## 2.1 Modeling

Though much of the discussion of jetting up to this point has been centered around pressure, a more useful metric for evaluating performance is power, as it factors in both size and speed of the jet simultaneously. Mitragotri et al. performed a study on the relationship between jetting power and delivery efficiency—the ratio of expelled volume to retained volume—in skin. Their findings suggest that high efficiency is assured in skin tissue above a delivery power of approximately 30W [74][75].

Accordingly, it is expected that each GI tissue will have inherent power requirements for depot formation—a metric that will be essential to understand before implementing any ingestible jetting device. However, before these power requirements can be characterized, a mechanistic model of a jetting system must be built, so that the jetting power can be precisely defined for a given a set of experimental input parameters. **Figure 2.1** describes the setup of this mechanistic model and is labelled with key parameters. Note that this model is similar to that developed in [76].

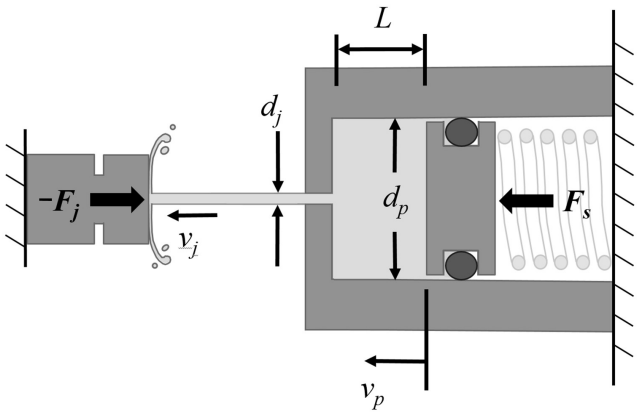


**Figure 2.1:** Diagram of a spring-powered jetting system.

### 2.1.1 Spring Model

It is assumed that energy in a jetting system is stored through compression of a spring. Such a spring could be pneumatic, metallic, or polymeric. Regardless of its type, the spring will apply a stored compression force, $F_s$, prior to jet expulsion, and "dead" compression force, $F_d$, after jet expulsion. $\alpha$ is defined as the fraction of the initially stored force applied by the final dead force in the jetting system. Thus,

$$\alpha = \frac{F_d}{F_s} \tag{1}$$

For pneumatic systems, $\alpha$ can be tuned by adjusting the ratio of final gas volume to initial gas volume. For metal spring-based systems, the manufacturer spring constant is used to control $\alpha$. The spring constant, $k$, of the system can be related to other system parameters as follows:

$$k = \frac{F_s - F_d}{L} = F_s\left(\frac{1-\alpha}{L}\right) \tag{2}$$

where $L$ is the stroke of the system (length of the ampule containing the payload fluid).

### 2.1.2 Energy

The energy initially stored in the system, $E_s$, (before jet expulsion) is

$$E_s = \frac{1}{2} k {x_s}^2 \tag{3}$$

where $x_s$ is the overall spring deflection in the stored state. In a practical jetting system, $\alpha > 0$ , which means that there is still energy stored in the spring after jet expulsion. This is the "dead" energy in the system, $E_d$, and can be calculated as follows:

$$E_d = \frac{1}{2} k {x_d}^2 \tag{4}$$

where $x_d$ is the spring deflection in the expelled state. The energy that is imparted upon the jetting fluid by the spring during the expulsion event, $E_{in}$, is the difference between the initially stored energy, and the dead energy.

$$E_{in} = E_s - E_d \tag{5}$$

$$E_{in} = \frac{1}{2} k ({x_s}^2 - {x_d}^2) \tag{6}$$

This can be algebraically rearranged as follows:

$$E_{in} = \frac{1}{2} L F_s (\alpha + 1) \tag{7}$$

According to the conservation of energy, the output energy $E_{out}$, should be equal to the energy input above. However, as will be discussed later, some energy will be lost to the friction imparted by the piston's sliding and the nozzle.

### 2.1.3 Bernoulli's Equation

Bernoulli's equation is an energy balance for fluid flow. The equation is defined as follows:

$$p_{in} + \frac{1}{2} \rho {v_{in}}^2 + \rho g h_{in} = p_{out} + \frac{1}{2} \rho {v_{out}}^2 + \rho g h_{out} \tag{8}$$

Where $\rho$ and $g$ are the fluid density (1000kg/m$^3$ in the case of water) and gravitational constant (9.8m/s$^2$ on Earth) respectively. $p_{in}$ is the inlet pressure, $v_{in}$, the velocity of the fluid at the inlet, and $h_{in}$ the elevation of the inlet with respect to the ground. The corresponding symbols on the

right hand side of the equation with the "out" subscript are for the system outlet. The Bernoulli equation also assumes that the flow rate, $Q$, between outlet and inlet is always constant. Thus, in the context of jetting,

$$Q = A_p v_p = A_j v_j \tag{9}$$

where $A_p$ and $A_j$ are the cross-sectional areas of the piston and jet respectively, $v_p$ is the velocity of the piston, and $v_j$ is the velocity of the jet as it exits the nozzle.

Note that at the inlet of a jetting system, pressure is imparted by the spring and piston, and at the output, no pressure is applied. Furthermore, input kinetic energy and gravitation throughout the system can be neglected given the scale of the system. Thus, for jetting systems, the Bernoulli equation becomes:

$$p_p = \frac{1}{2}\rho {v_j}^2 \tag{10}$$

Where $p_p$ is the pressure applied by the piston. If friction is neglected, the pressure imparted by the piston is defined as follows:

$$p_p = \frac{F_s - kx_p}{A_p} \tag{11}$$

Where $x_p$ is the position of the piston with respect to its starting location and $A_p$ is the area of the piston. Given the above equations, the Bernoulli energy balance becomes:

$$\frac{F_s - kx_p}{A_p} = \frac{1}{2}\rho\left(\frac{A_p}{A_j}v_p\right)^2 \tag{12}$$

$$F_s = k \cdot x_p + \frac{1}{2}\rho\frac{{A_p}^3}{{A_j}^2}{v_p}^2 \tag{13}$$

### 2.1.4 Dynamics

At this point, it is useful to explicitly state time-dependent terms, so system dynamics can be resolved. It is also worth grouping constants to simplify the expression:

$$F_s = k \cdot x_p(t) + C_1 \cdot \left(v_p(t)\right)^2 \tag{14}$$

where

$$C_1 = \frac{1}{2}\rho \frac{{A_p}^3}{{A_j}^2} \tag{15}$$

Because the velocity of the piston is the derivative of its position, the energy balance can be written as a differential equation:

$$0 = k \cdot x_p(t) + C_1 \cdot \left(\frac{dx_p(t)}{dt}\right)^2 - F_s \tag{16}$$

The boundary condition $x_p(0) = 0$ is applied, and it is assumed that the time required for acceleration of the piston is negligible (i.e. the velocity boundary condition is "free" at t = 0). Solving the above first-order nonlinear differential equation yields two equations for $x_p(t)$. Since all constants are positive, solutions that would result in a negative position can be ignored. Thus the following solution is obtained:

$$x_p(t) = t\sqrt{\frac{F_s}{C_1}} - \frac{k}{4C_1}t^2 \tag{17}$$

With the above equation, the time point at which all of the fluid is expelled can be determined by solving for $t_{max}$, where $x_p(t) = L$:

$$L = (t_{max})\sqrt{\frac{F_s}{C_1}} - \frac{k}{4C_1}(t_{max})^2 \tag{18}$$

Of the two solutions yielded by the above substitution, the solution which must always be positive is selected as this work only considers systems with positive time-points and parameters:

$$t_{max} = \frac{2}{k}\left[\sqrt{C_1 F_s} - \sqrt{C_1(F_s - kL)}\right] \tag{19}$$

Velocity of the piston, $v_p(t)$ can also be resolved by taking the derivative of $x_p(t)$:

$$v_p(t) = \frac{dx_p(t)}{dt} = \sqrt{\frac{F_s}{C_1}} - \frac{k}{2C_1}t \tag{20}$$

Applying conservation of flow, the velocity of the jet is:

$$v_j(t) = \frac{A_p}{A_j} v_p(t) \tag{21}$$

The equation for nozzle thrust [77] can be applied to determine the force applied by the jet at the orifice.

$$F_j(t) = \rho Q v_j(t) \tag{22}$$

$$F_j(t) = \rho A_j \left(v_j(t)\right)^2 \tag{23}$$

The power of a jet of fluid, $P_j$, is defined as follows:

$$P_j(t) = \frac{1}{2}\dot{m}\left(v_j(t)\right)^2 \tag{24}$$

Where $\dot{m}$ is the mass-flow rate. This equation can be re-written in either of the following ways:

$$P_j(t) = \frac{1}{2}\left(\rho A_j\right)^{-\frac{1}{2}}\left(F_j(t)\right)^{\frac{3}{2}} \tag{25}$$

$$P_j(t) = \frac{1}{8}\cdot\rho\cdot\pi\cdot {d_j}^2\cdot v_j(t)^3 \tag{26}$$

Where $d_j$ is the diameter of the jet. Equation (25) is most useful for resolving jet power from measured force data (as will be done in **Sub-section 2.4**), while equation (26) is a commonly employed expression for resolving jetting power based on observed velocity [74][75].

It is also useful to be able to quickly calculate the power output, given a known pressure input and orifice size. This can be accomplished by combining equation (10) and equation (26):

$$P_j = \frac{1}{2\sqrt{2}} \cdot \pi \cdot {d_j}^2 (\rho)^{-\frac{1}{2}} \cdot \left(p_p\right)^{\frac{3}{2}} \tag{27}$$

The total energy contained within the jet, $E_{out}$, can be obtained by integrating the power equation over the duration of the jetting event. Given that no losses were included in the above analysis, $E_{out}$ is equal to $E_{in}$ from the spring input.

$$E_{out} = \int_0^{t_{max}} P_j(t) \cdot dt \; = \frac{1}{2} L F_s (\alpha + 1) \tag{28}$$

### 2.1.5 Losses

In order to improve the accuracy of the model, friction loss from the piston, and nozzle efficiency loss are considered. In this section use of the subscript "ideal" denotes ideal quantities, as they were defined in previous sections. The subscript "real" denotes quantities from the previous sections with losses now considered. An absence of these subscripts means the parent quantity is the same for a system with and without losses considered.

Friction loss from the piston can be represented as a force opposing the spring force at all-time points. Thus, the pressure term becomes:

$$p_{p,real} = \frac{F_s - k x_p - F_f}{A_p} \tag{29}$$

Where $F_f$ is considered constant and can be determined empirically. Thus $F_s$ and $F_f$ can be combined into one quantity, $F_{s,real} = F_{s,ideal} - F_f$. All instances of $F_s$ in the theoretical equations of motion from the previous section can be replaced by $F_{s,real}$ to account for the friction loss.

Note that the piston friction applies a force over the duration of the stoke. Thus some of the input energy is expended to drive the piston. The energy input becomes

$$E_{in,real} = E_{in,ideal} - L F_f \tag{30}$$

The above equation can be employed to generate a single coefficient, $\eta_f$, that can be used to assess the impact of friction on the efficiency of the system:

$$\eta_f = \frac{E_{in,real}}{E_{in,theo}} = 1 - \frac{2F_f}{F_s(1+\alpha)} \tag{31}$$

In addition to friction losses, nozzle losses are considered. These losses occur from flow converging and interacting with the nozzle surfaces. There are many ways to model and account for such losses, but for the purposes of this work, it will be assumed that there is a net efficiency applied to the input energy imparted on the fluid. As such, this efficiency would need to be measured prior to application of the model.

The nozzle efficiency is denoted as $\eta_n$, and can be incorporated into the grouped-constant, $C_1$, from the previous section as follows:

$$C_{1,real} = \frac{1}{2}\frac{\rho {A_p}^3}{\eta_n {A_j}^2} \tag{32}$$

$\eta_n$ likely varies based on the Reynolds number of the jet, geometry of the nozzle, and other parameters and variables, but in this work a single, empirically determined value is applied across all nozzle sizes and flow conditions.

Lastly, applying losses to equation (27) can result in a more accurate prediction of power output as it relates to input force or pressure:

$$P_{j,real} = \frac{1}{2\sqrt{2}} \cdot \pi \cdot {d_j}^2 (\rho)^{-\frac{1}{2}} \cdot \left(\eta_n \frac{F_{s,real}}{A_p}\right)^{\frac{3}{2}} \tag{33}$$

Note that in this loss model, it is assumed that diameter of the jet remains equal to that of the orifice (ignoring factors such as velocity and diameter coefficient).

### 2.1.6 Sample Model Outputs

The above equations were employed to generate theoretical performances for various nozzles at a fixed initial force $F_s$ = 66 N and $\alpha = 0.45$. Piston friction was measured to be 4 N, and an efficiency of 80% was assumed for all nozzles.

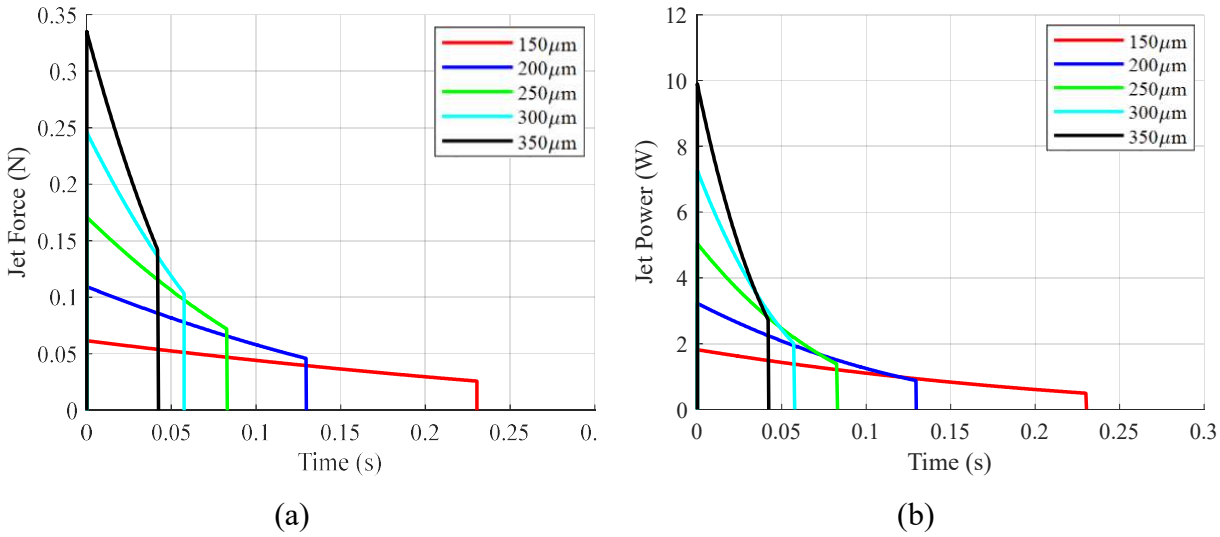


**Figure 2.2:** Theoretical jetting performance over range of nozzle orifice sizes. (a) Force (b) Power

Note that increasing nozzle diameter results in a greater peak power (though the area under the curve remains the same). Thus increasing nozzle diameter may result in deeper tissue penetration, even though the net energy expenditure is the same. Alternatively, the peak power could be increased by increasing $F_s$. As was noted earlier, it will be important to understand the relationship between these design parameters and tissue penetration in order to implement an ingestible jetting device. (This will be explored in **Chapter 3**.)

A MATLAB implementation of the above model can be found in **Appendix IV**.

## 2.2 Experimental Methods

In order to validate the above model so that it may be used with confidence, jetting performance data was collected using a custom jetting system and commercial force transducer.

### 2.2.1 Testing apparatus

The test-stand was designed to measure jetting force while varying parameters including nozzle orifice size, initial and final spring force, standoff distance, fluid viscosity, angle of incidence, and expelled volume. The main component of the test stand is a hand-held jetting device mounted onto an aluminum rail. Also mounted to the rail is a linear stage and force transducer (see **Figure 2.3**).

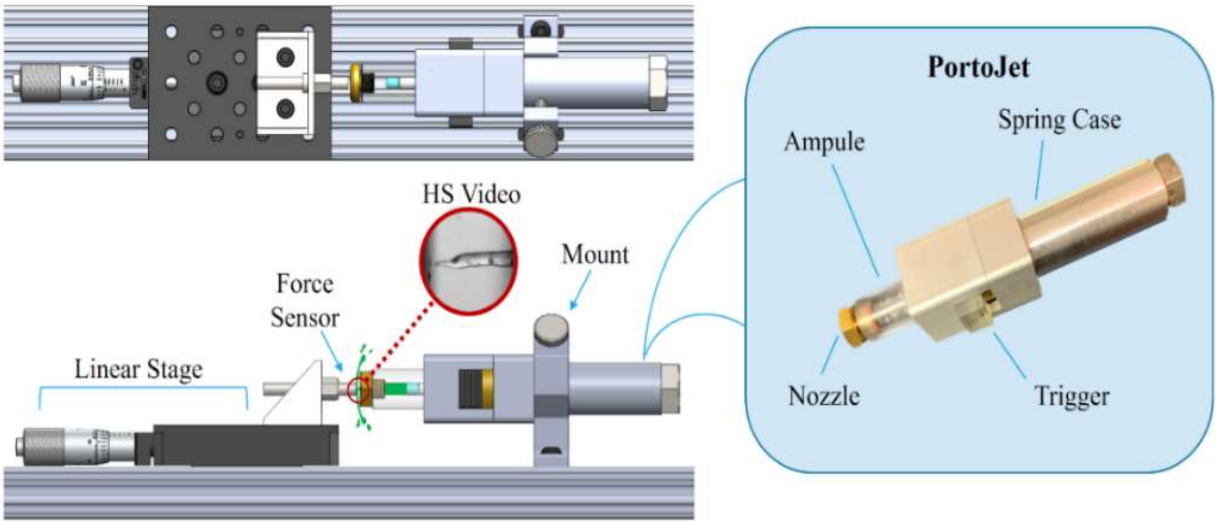


**Figure 2.3:** Testing apparatus used for validating jetting performance, including handheld device, "PortoJet"

The hand-held device, referred to as "PortoJet" can be mounted to and removed from the rest of the test stand easily. This allows for quick refilling of the fluid ampule between trials. The operator may also choose to remove the PortoJet to quickly switch nozzles, and springs if desired.

Load can be applied in the PortoJet either by a pneumatic cylinder or a spring. Use of a pneumatic cylinder is generally preferable for experimentation as spring design inputs can be easily adjusted. For example, the initial force, $F_s$, applied by the pneumatic cylinder is a function of the cylinder pressure—which can be quickly changed via a pressure regulator. Furthermore, the final spring force (or α-value) of a pneumatic cylinder can be adjusted by simply re-defining the initial position of the pneumatic piston with a spacer. This is far simpler than purchasing a new spring for every load condition.

That said, for the work described in this section, it was only necessary to use one spring force to assess the accuracy of model. Thus a coil spring with $F_s = 66$ N and $\alpha = 0.45$ was employed. The different configurations of PortoJet (spring and pneumatic) can be seen in **Figure 2.4**.

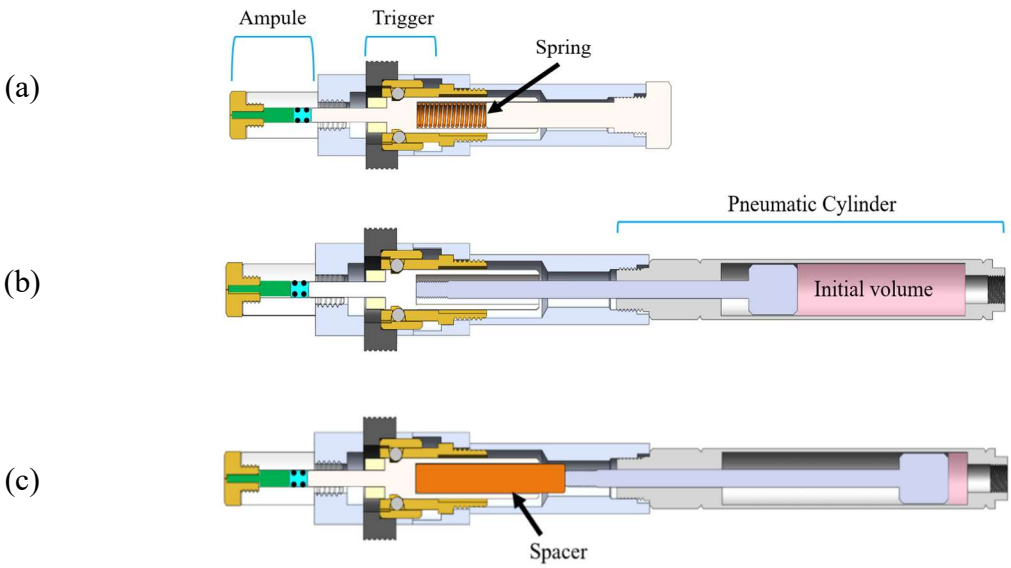


**Figure 2.4:** Diagram showing section views of different versions of the PortoJet (a) With spring. (b) With pneumatic cylinder containing large initial volume, resulting in high α-value. (c) With pneumatic cylinder containing low initial volume, resulting in low α-value.

It was also important to devise a triggering mechanism for the PortoJet which accurately represented that of a potential ingestible device. As such, the trigger needed to withstand large loads, and be able to release these loads quickly. A repurposed Parker quick-disconnect hose fitting, was found to excel at these functions.

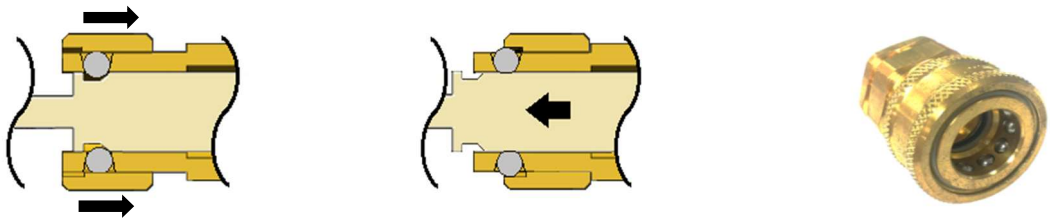


**Figure 2.5:** Triggering mechanism for PortoJet (a) in the loaded state; (b) in the released state. (c) Parker quick-disconnect fitting on which the triggering mechanism was based [78]

As the sleeve of the fitting is retracted, the ball bearings are allowed to move radially outward. An internal rod, which was axially constrained by the balls, is therefore allowed to translate, and apply a load to the ampule (see **Figure 2.5**). This design has proven successful in

satisfying the loading and release requirements for this work, though other solutions can be found in commercial needleless injectors.

### 2.2.2 Data collection

The sensor used was a Kistler 9215A piezoelectric force transducer that interfaces with a Kistler 5165A4KH10 LabAmp® Dynamic Laboratory Charge Amplifier. The amplifier was connected to a Windows 10 laptop via Ethernet, and data acquisition was triggered via Kistler's web-browser based interface. The total acquisition time used for trials was two seconds at a sampling frequency of 20kHz.

Although high-speed video was used during tests, it was deemed to be less than ideal due to the fact that discrete elements of fluid were not observable after jetting initiated. Having said that it is possible to employ high-speed video to verify the total time of a jetting event (as will be shown in **Section 4.5**). Furthermore, high-speed video is useful for observing the shape of the jet to verify that the jet is indeed columnar and not a spray.

Five replicates were performed for each experimental data point. An ampule volume of 200uL (6 mm diameter and 7 mm stroke) was used for all experiments. 100% deionized water was used for all tests except for those in which fluid viscosity was varied.

## 2.3 Data Processing

Each data-set, containing 40000 individual time-points, was imported into MATLAB. From there, the maximum load measurement of the data set (assumed to be the peak force applied by the jet) was extracted. Next, the time at which jetting began was determined based on the point at which the measured force exceeded 10% of the peak. Likewise, the time that jetting ceased was marked when the measured force returned below the same threshold.

It was observed, through use of MATLAB's Fast Fourier Transform function, that data-sets contained high-frequency oscillations at ~35kHz. This was assumed to be sensor noise as the oscillations swung into both the positive and negative range in the time domain. This noise was removed by use of a moving average filter with a half-width of 5ms.

Sensor drift resulted in a linear decay in measured force of approximately 0.1% per millisecond of applied static load (as reported by the manufacturer). This drift is the result of loss in charge within the piezoelectric sensor, which is designed mainly for dynamic loads. As such, compensation was applied to each dataset to correct for the drift.

After filtering and drift correction, replicates were combined to create an estimate for mean performance with 95% uncertainty. With the output data, equations from **Section 2.1** were used to generate estimates of nozzle efficiency for each orifice size.

## 2.4 Experimental Results

Results were plotted for each experiment performed. In each case the nozzle efficiency was deduced by comparison with the theoretical energy input into the jet (i.e. minus piston friction).

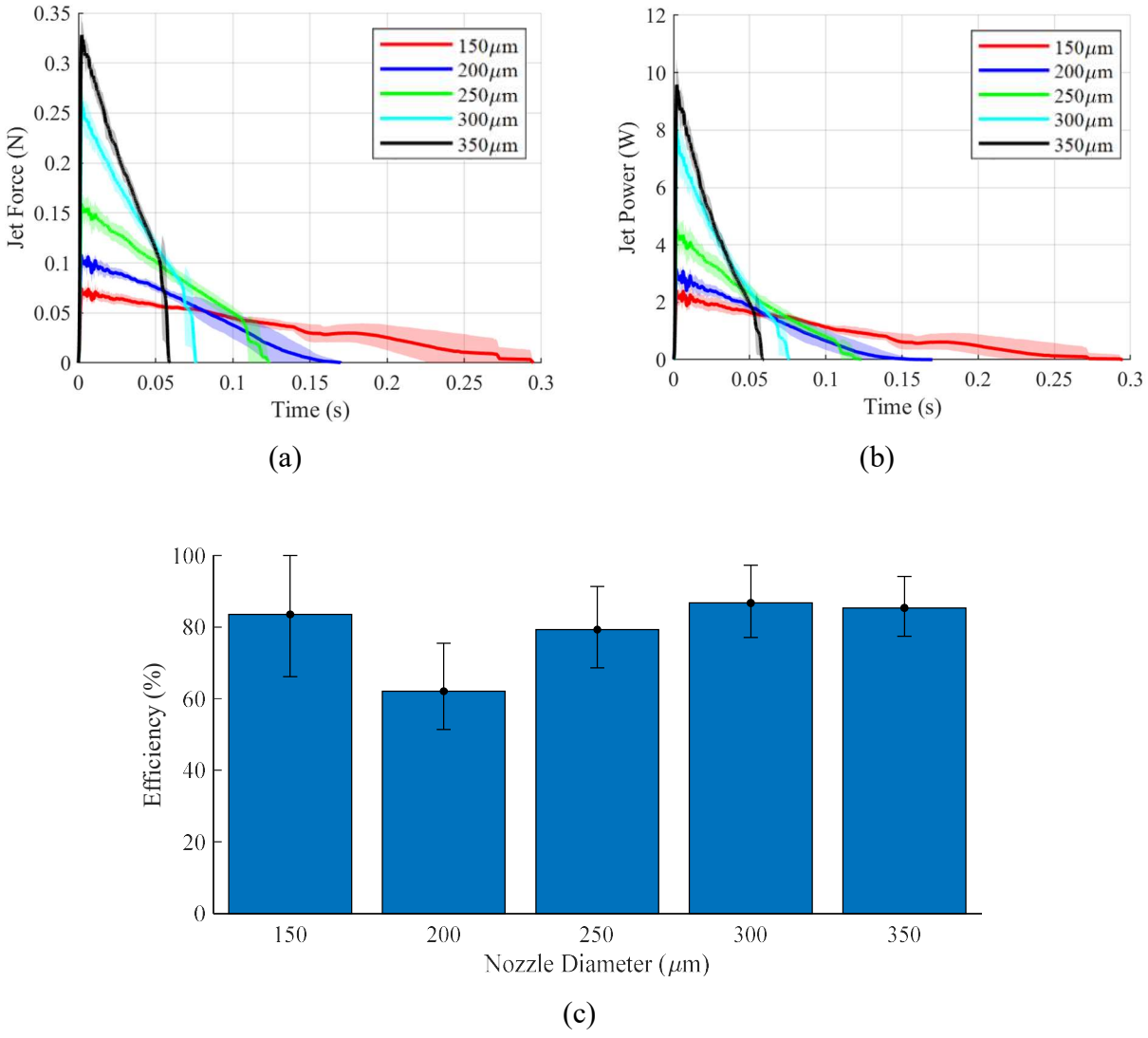


**Figure 2.6:** Experimental jetting performance over range of nozzle orifice sizes. (a) Force data – each curve is mean of n=5 replicates and shaded regions are 95% confidence interval. (b) Resolved experimental power data (c) Nozzle efficiencies given theoretical energy input. NOTE: the experimental data displayed in this figure was collected using a variant of PortoJet developed by Novo Nordisk.

A comparison between **Figure 2.2** and **Figure 2.6** shows that the theoretical model agrees with the measured data. In general, efficiencies fall between 75 and 85% (though, for the 200 μm nozzle, the efficiency was approximately 60%). Nozzle efficiency for any jetting device should be measured prior to implementation of other design features as it can greatly impact performance. It is worth noting that efficiencies can be improved by altering the geometry and surface roughness of the nozzle however, such improvements were considered beyond the scope of this work.

# 3 Tissue Characterization

As noted in **Section 1.2**, previous ex-vivo work with jetting systems has yielded an extensive body of data on penetration characteristics of jets on skin tissue. However, little to no data exists for jetting in the GI tract. For the purposes of this study, submucosal injection—where a depot is formed directly beneath or within the submucosal tissue—was targeted. Although intramuscular delivery is also feasible in some GI organs, in others, the muscular layer is too thin to support a sizeable payload without risking perforation.

No models that describe the penetration of GI tissue by jets could be located. Aran et al. modeled jet-based penetration of the mucous layer with computational flow analysis [22], but this would likely be insufficient for predicting deeper penetration. Given the complexity of developing an accurate tissue model, this was considered beyond the scope of this thesis. That said, this thesis hypothesizes that power requirements for forming depots in the GI tract are lower than that of skin.

## 3.1 Ex Vivo Experimental Methods

The goal of the ex vivo experiments is to measure jet interactions with GI tissue, such as delivery efficiency and penetration wound size. These tests were performed on a variety of GI tissues including those of the cheek, esophagus, stomach, large intestine, and rectum. Tissue was tested within six hours of excision. As necessary parameters for delivery were not known initially, a trial and error-based screening was performed to identify a starting point for each tissue type. The data collected from these experiments will provide a preliminary empirical basis for achieving high delivery efficiency, as well as a sense of the impact that jets have on mucosal tissue.

### 3.1.1 Testing Apparatus

The PortoJet system was used to inject 200uL of contrast agent or histology dye into 5 x 5cm samples of porcine GI tissue. A pneumatic cylinder with an α-value of 0.90 was used for power in all tests. The PortoJet was mounted vertically and tissue was placed directly beneath it on a foam base. The tissue was then brought into contact with the jet nozzle using a scissor jack.

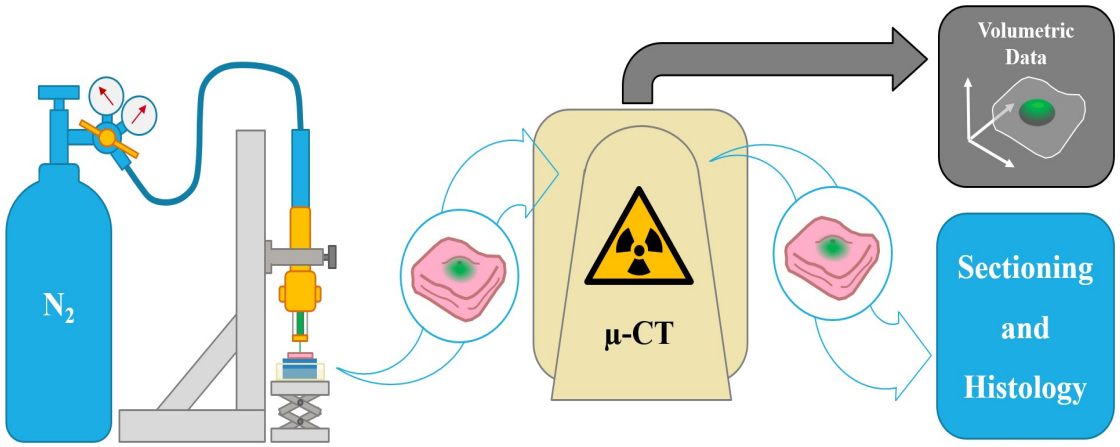


**Figure 3.1:** Experimental work-flow for ex vivo tissue testing and imaging

### 3.1.2 X-ray Microtomography

X-ray microtomography (micro-CT) was used to analyze the volumetric efficiency of delivery for each sample. A suspension of 5% wt. barium sulfate was employed as a contrast agent for injection. Tissue samples were scanned within ten minutes of injection so that diffusion was minimized prior to evaluation. The Micro-CT machine captures 2D slices of the tissue with x-ray. A post-processing program was used to reconstruct these slices into a 3D matrix (with high-intensity voxels associated with less light transmission). A threshold is selected manually, and all voxels above this threshold are considered delivered volume.

### 3.1.3 Histology

A collection of injection trials was performed for histology. In these trials, the tissue was injected with fluorescent dextran. Tissue was frozen at -80ºC and later sectioned at -20ºC in a cryostat with a microtome. Samples were photographed with UV microscopy.

## 3.2 Ex Vivo Results

**Figure 3.2** shows sample micro-CT measurements with successful depots for a variety of tissue types. Depots were observed in all organs except for the esophagus.

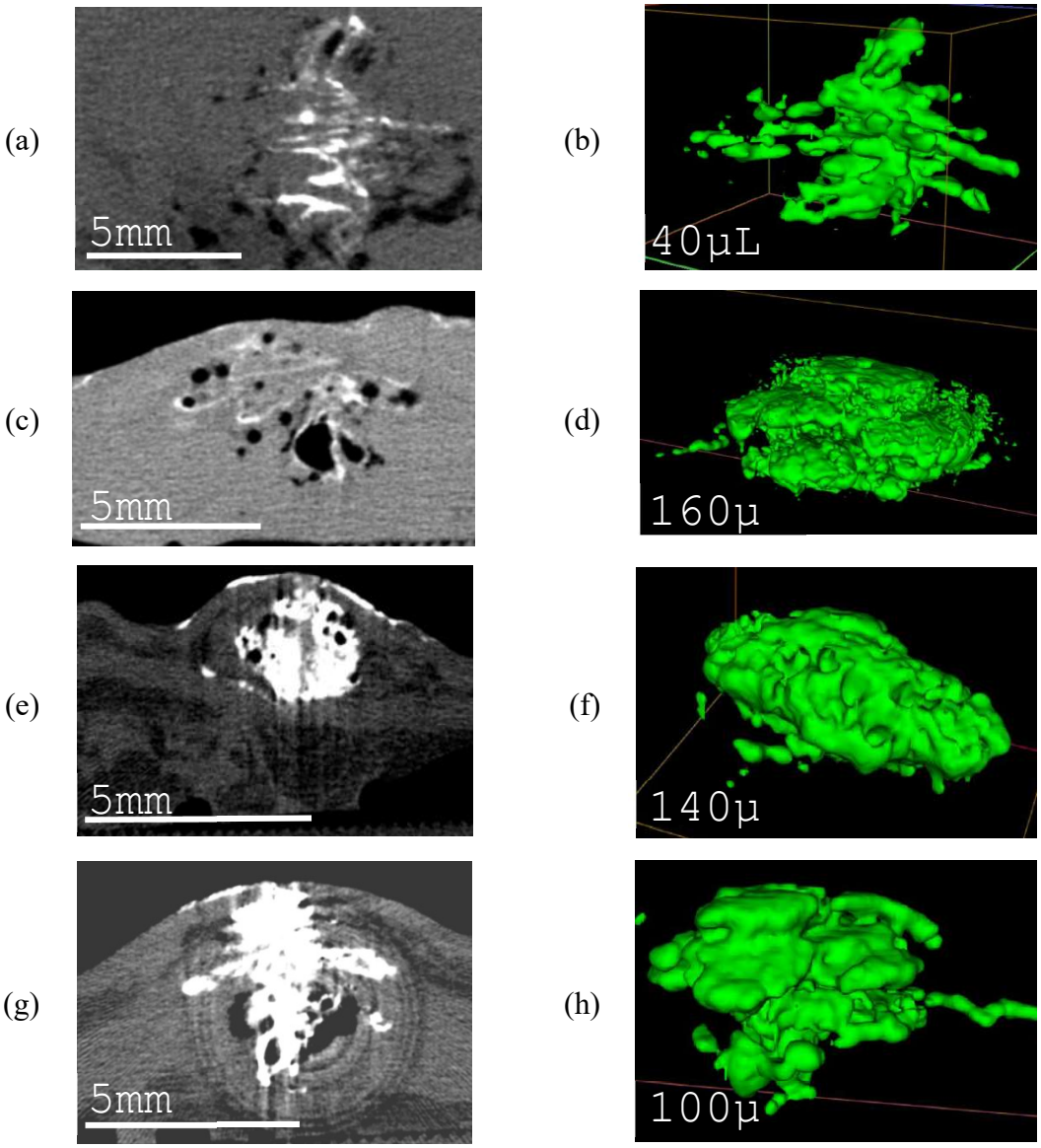


**Figure 3.2:** Micro-CT images of depots in GI tissue after 200µL jet injections – cross sections on left, volumetric rendering on right. (a)(b) Cheek: $d_j$ = 350µm, $F_s$ = 236N. (c)(d) Stomach: $d_j$ = 350µm, $F_s$ = 177N. (e)(f) Colon: $d_j$ = 350µm, $F_s$ = 47N. (g)(h) Rectum: $d_j$ = 350µm, $F_s$ = 98N.

From the micro-CT images, it is clear that air bubbles (represented by dark-spots), are present in the center of each depot. It is not clear how these bubbles form, although cavitation could be an explanation. While these air pockets do not interfere with the delivery efficiency

analysis, they could be of concern from the perspective of safety. As such, further analysis of air cavities in the context of safety will be essential prior to translation of this technology into a clinical or market setting. Use of a different contrast agent could be considered as the barium-sulfate contrast agent is a non-homogeneous suspension rather than a solution (which could affect results).

The above micro-CT data was useful for verifying delivery efficiency. However, from this data, it is not possible to discern tissue layering and structures. To that end, histology is more useful. **Figure 3.3** shows preliminary histology data on stomach tissue.

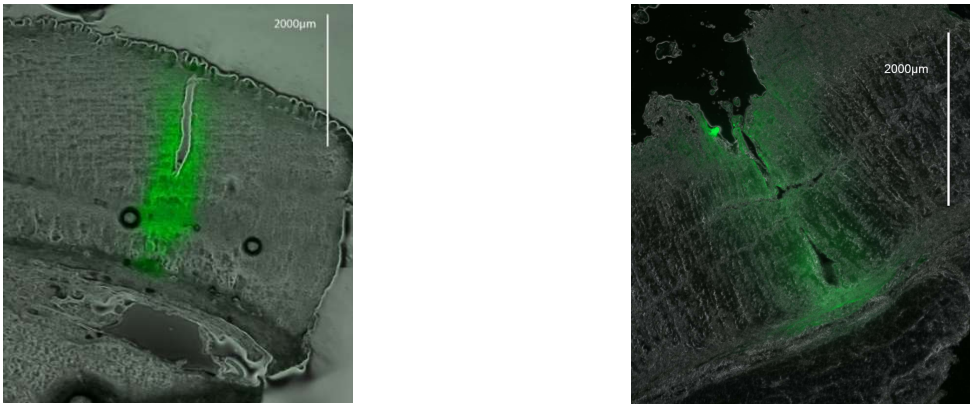


(a) (b)

**Figure 3.3:** Histology of stomach tissue after delivery of 40µL of fluorescently marked dextran. (a) Penetration of the mucosal layer with visible wound. (b) Deep penetration with absorption into of the submucosa visible.

Absorption into the mucosa as well as the submucosa is visible. Also, note the clear penetration wounds, each between 0 and 500µm in diameter and traversing the depth of the entire mucosa. Clearly jets create an observable wound, though this wound is smaller than those seen in mili-needle systems [27]. Also, in these particular trials a volume of 40µL was employed and as a result, depots are less apparent than would be expected for the micro-CT trials (which employed 200µL doses).

Using this histology data, as well as the micro-CT data, a semi-quantitative summary of jetting performance in the GI tract was created (shown in **Figure 3.4**). This data should provide a sense of which input jetting parameters will result in depots across multiple tissue types.

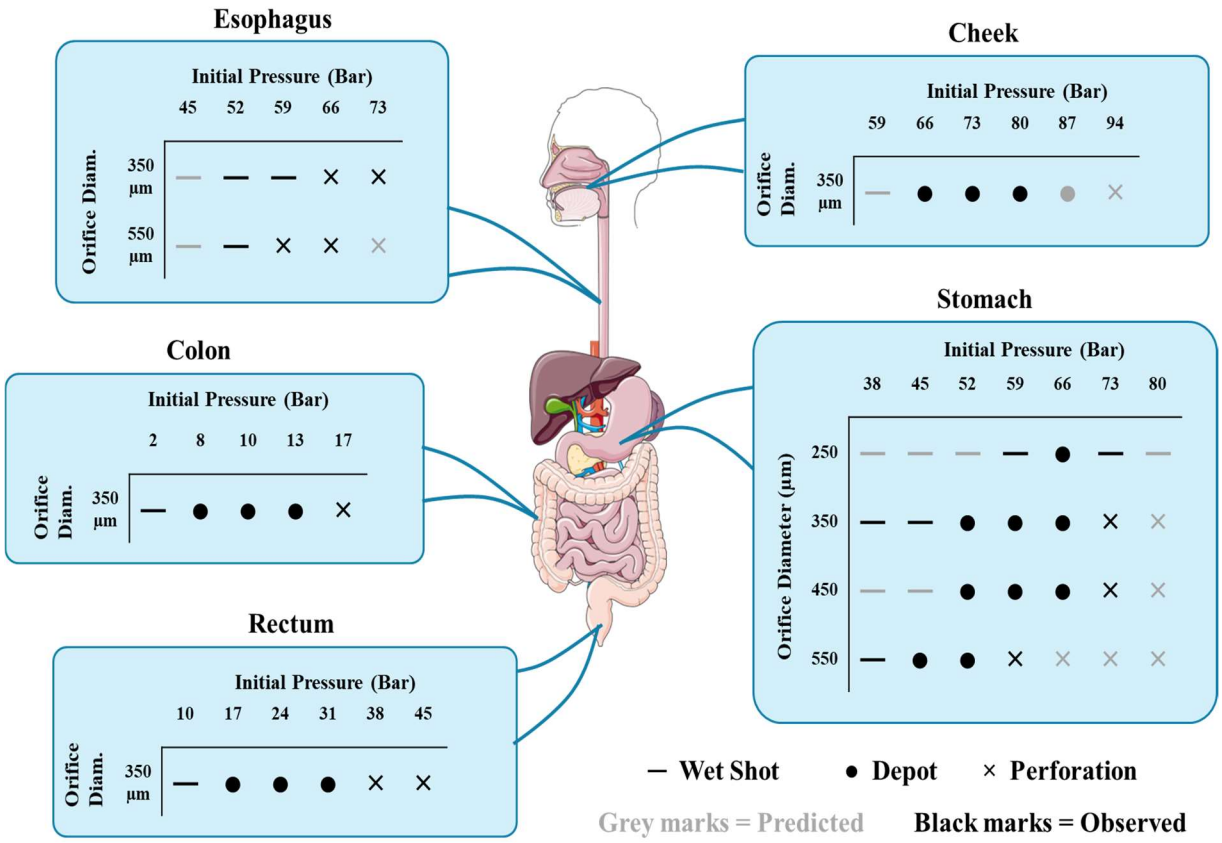


**Figure 3.4:** Preliminary summary of peak jetting pressure performance across multiple tissue types (n = 1 for all points). NOTE: initial pressures were corrected for piston friction losses. Also, despite the diagram, human tissue was not used (but rather porcine tissue).

"Wet shots" refer to trials where most liquid was observed to be on the surface; "Depot" means a visible depot was observed both visually and through micro-CT; and "Perforation" means a clear wound was visible on the serosal side of the tissue and little to no contrast agent was contained within.

Equation (33) was used to calculate the minimum observed peak power requirement for each organ based on the data in **Figure 3.4**. The results are tabulated in **Table 3.1**. It is important to note that lower minimum requirements might be possible given smaller nozzle sizes which were not tested in this work.

**Table 3.1:** Summary of minimum peak power requirement for forming depots in GI tissue (corrected with $\eta_n = 0.80$)

| Organ | Min. pk. power to achieve depot |
|---|---|
| Cheek | 52W |
| Esophagus | - |
| Stomach | 26W |
| Colon | 2W |
| Rectum | 7W |

The power required to achieve a depot in each tissue type varied widely from organ to organ. However, as hypothesized, the minimum peak requirement in most GI organs appears to be lower than that of skin (i.e. 30W, according to [75]). No depots were observed in the esophagus. However, depots could be possible at orifice diameters which were not measured.

More work is currently underway for the purposes of adding fidelity to each measurement and covering additional organs (such as the small intestine) which were omitted due to time constraints.

# 4 Device Development

Equipped with an ability to precisely define device jetting power output, as well as a knowledge of jetting power requirements for depot formation in GI tissue, movement towards a device design is possible. The following chapter includes discussion of additional requirements for an ingestible jetting device, implementation of device concepts to meet requirements, and testing that was carried out to evaluate the performance of devices. The work here represents one of many possible ingestible jetting devices and should be considered a proof of concept rather than a final design.

## 4.1 Engineering Requirements

The first step of any design effort is to define requirements. Up until now, this thesis ha mainly discussed jetting power as a requirement. However, a host of other requirements exist that must be satisfied in order to ensure safe and efficacious implementation of a jetting device.

### 4.1.1 Avoidance of Obstruction

An obstruction occurs when a device is permanently lodged at some location in the GI tract, disrupting the normal passage of digested matter, and potentially resulting in abrasion, ulceration, tissue necrosis, or the stifling of nutritional uptake. Such obstructions have been reported in studies of slow-release osmotic pumping systems, and are usually attributed to the size of the device. Larger devices are more likely to cause an obstruction resulting in a need for medical intervention [79]. As such, minimizing device size as much as possible is desirable from a safety perspective. As an aside, minimizing device size could also help with adherence, as patients are more likely to adopt a smaller pill [80].

### 4.1.2 Reduction of Trauma

Trauma at the injection site is also of great concern for a jetting device. At the location where the depot is formed, it is clear that the submucosa will be lifted away from the muscularis. Furthermore, there are capillaries running through the submucosa which could be damaged and/or hemorrhage, resulting in infection at the injection site. Aside from infection, if the jet is too strong, it could perforate the muscularis, leading to contamination of the paratenium by gut bacteria (paratenisis). Although there is no data on the above safety issues for GI based jetting systems, it is probable that minimizing jet diameter and payload volume would decrease the risk of trauma. However, the true safety impact of trauma in GI tissue due to jetting is not understood and should be investigated further.

### 4.1.3 Minimization of Delivery Failures

Delivery failure presents yet another potential safety issue for jetting devices (though one which depends largely on the intended use of the therapeutic). If the jet does not penetrate to the proper depth and deliver the desired dose, this would result in a diminished or non-existent therapeutic effect. There are multiple reasons why delivery failure might occur. For example, food debris could interrupt the transit of the jet or the device orifice could be misaligned relative to the tissue. For certain biologics, such as vaccines or allergens, occasional delivery failure could be permissible. However, for therapeutics where immediate dosing is essential (such as insulin for glycemic control, or epinephrine for anaphylaxis), a missed dose could be life-threatening. There are numerous strategies that could be taken to avoid dosing failures, some of which include tissue contact sensing, self-orientation, and mucoadhesives.

### 4.1.4 Use of Non-toxic Materials

Acute and chronic material toxicity of the device must be taken into consideration. For example, if the device were made of aluminum, chronic absorption of metabolized device materials could lead to aluminum poisoning [81]. Generally speaking, toxicity concerns can be mitigated by employing materials that are bio-inert or otherwise non-toxic (e.g. titanium, PDMS, PCL, salts, carbohydrates). Polymeric or non-reactive metallic coatings could also be used to protect the device from degradation. Examples of materials thought to be safe for ingestible devices are described by Bettinger et al. [82].

### 4.1.5 Shelf-life

The sponsor of this research specified that it is generally desirable to target a minimum shelf-life of two years for therapeutics. Though the shelf-life typically depends on the payload formulation properties, certain design features of the device itself could also affect shelf life. For example, a degradable component might necessitate that the device be stored with a desiccant. Furthermore, a device containing a sealed gas cavity might require additional measures to stifle gas diffusion. Also, ampule materials could interact with the biologic formulation, resulting in degradation.

## 4.2 System and Sub-system Concepts

Keeping all of the above requirements in mind, it is possible to select mechanical design concepts for an ingestible jetting device. Though multiple system and sub-system concepts were explored, it was determined that a passively triggered self-orienting device for use in the stomach was most promising. The following section describes the rationale for selecting such a design, as well as design details.

### 4.2.1 Target Organ: Stomach

The stomach is an attractive target organ for multiple reasons. For one: a device would enter the stomach within seconds of ingestion and remain there for multiple hours thereafter. This means that a timed trigger could be implemented for release of the jet in the stomach, whereas for GI organs distal to the stomach (SI, colon, rectum) there is much greater uncertainty as to when triggering should occur (see **Table 1.3**).

Aside from timing, the stomach does not transmit acute pain sensation [83], meaning an injection in the stomach would likely go unnoticed by a patient. In the esophagus or cheek, an injection would almost certainly be felt by the patient. Furthermore, stomach tissue is relatively thick, so minor variation in jetting performance due to manufacturing tolerances would be less likely to result in perforation. Lastly, the sterility of the stomach is high due to the presence of stomach acid.

It is also worth noting potential drawbacks of targeting the stomach. For one, delivery in stomach tissue requires a minimum peak power that would cause perforation in distal GI organs. This could pose a safety risk if the device were inadvertently triggered after passage through the stomach. Aside from this, food debris is more likely to be present in the stomach, and could

interfere with jetting performance. That said, these potential downsides of gastric jetting are speculative as this technology has yet to be assessed in a clinical setting.

### 4.2.2 Tissue Localization: Self-orientation

Another important design consideration is tissue localization—the means through which the functional feature of the device (in this case, the jet orifice) is guaranteed contact with the tissue. Robust tissue localization increases the likelihood of successful dosing.

Previous research efforts have reported a multitude of strategies for accomplishing tissue localization. Abramson et al. report the use of a self-orienting system for the stomach [27] while Rani therapeutics reports the use of a balloon structure for alignment in the small intestine [29]. For purposes of this study Abramson et al.'s self-orientation mechanism was an appropriate choice as the stomach was also selected as a target organ.

In a self-orienting system, a combination of geometry and mass distribution result in a system which is solely stable in an orientation that aligns the orifice with the tissue. For any free body, if the center of gravity (CG) is not directly above the body's point or line of contact with the ground, a net torque on the body will result. Designed properly, a self-orienting jetting device leverages this torque to roll in the direction of the orifice. When the device CG is directly above the orifice, there will be no torque on the device, resulting in a stable orientation. This process is described by **Figure 2.1**.

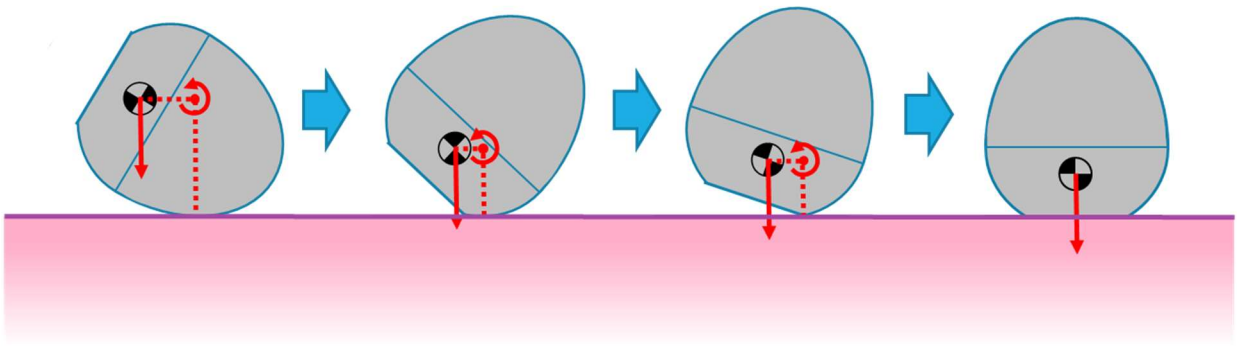

**Figure 4.1:** A self-orienting device

### 4.2.3 Power: Compressed Gas

As shown in **Table 3.1**, the minimum jetting power requirement to achieve depot formation in stomach tissue is approximately 26W. This corresponds to a power density requirement of approximately $3\times10^{-2}$ W/mm$^3$ (assuming the device is a sphere with diameter 12mm).

An electrically driven jet could be appealing for its controllability (as is accomplished by Portal Instruments' technology [84]). However, conventional batteries and supercapacitors have maximum power densities on the order of $2\times10^{-3}$ W/mm$^3$ [85], which is not sufficient to meet the above power density requirement. Having said that, batteries or capacitors could be used as a means for triggering a separate power unit such as a chemical reaction, as was described in WO2018049133 (A1) [26]. Alternatively, a tethered system with a large external battery or capacitive power unit could be used given a sufficiently small internal actuator.

Another potential option for power is a chemical reaction, which would generate a gas such as $CO_2$ to drive the jet. Such a reaction was demonstrated by Aran et al. in their MucoJet system [22]. However, the pressures developed within MucoJet (0.1 - 0.3 Bar) are orders of magnitude lower than the pressures required for penetration of stomach tissue at any reasonable orifice size (see **Figure 3.4**). Thus, it seems unlikely that the MucoJet mechanism could be applied for submucosal depot formation in the stomach.

Perhaps the simplest solution would be a mechanical spring such as the disk spring discussed in **Chapter 2**. However, it was found that the springs which were strong enough to satisfy the stomach's jetting power requirement interfered with the device's self-orientation properties (i.e. the springs were too heavy). That said, in a system targeting organs with lower power requirements, the spring's weight would have less of an impact on self-orientation. Also, for a non-self-orienting system, the spring weight would not be relevant.

In light of the above information, a compressed gas ($CO_2$) was used, as such a gas behaves much like mechanical spring, but is lightweight by comparison. In other words: use of a compressed gas allowed for meeting of the power requirement without sacrificing self-orientation. Compressed gas does have drawbacks though. For example, sealing a small pressure vessel could incur significant manufacturing cost as it would almost certainly mandate a metal lining and micro-welded interface to impede diffusion. Having said that, a brief evaluation of device sealing showed that gas leakage was sufficiently small for research purposes (see **Appendix III**).

### 4.2.4 Triggering: Sugar-Plug

For a device that targets the stomach, triggering should occur between five and twenty minutes after ingestion. Our triggering mechanism is composed of an isomalt "sugar-plug" which passively degrades in humid environments. This sugar-plug is placed directly in front of the orifice. Thus, the payload fluid, which is constantly pressurized, cannot escape from the chamber as it is blocked by the sugar-plug. To prevent the payload fluid from degrading the sugar-plug, the plug is separated from the orifice exit by a thin polymeric membrane.

When the device is ingested, the sugar-plug begins to dissolve. Eventually, it becomes thin enough so that the pressure exerted by the payload fluid ruptures the membrane and clears away any remaining isomalt. At this point, there is nothing obstructing the fluid from exiting through the orifice and a jet forms. This triggering process is illustrated in **Figure 4.2**.

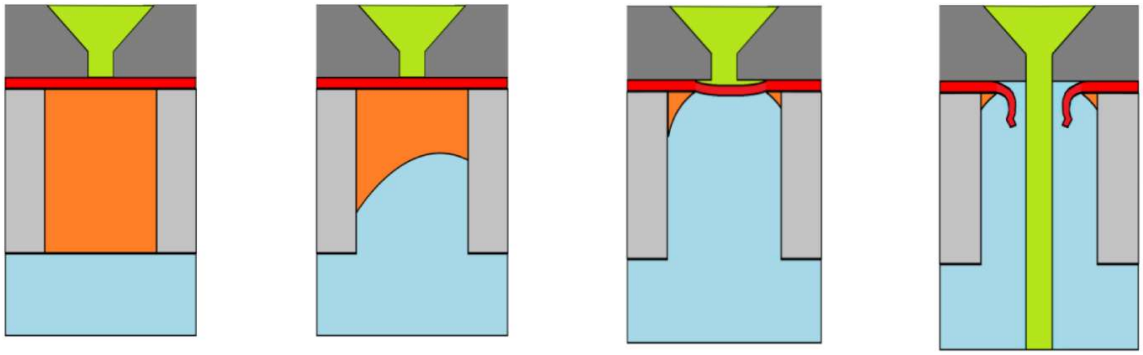


**Figure 4.2:** Diagram of the "Sugar-plug" triggering mechanism (a) in the pre triggered state; (b) as it begins to dissolve; (c) as the rupture film begins to deflect; (c) after rupturing and release of the jet. NOTE: the length of the sugar plug can be adjusted to increase or shorten triggering time.

## 4.3 Integrated Device Design

After a target organ, localization method, powering method, and triggering mechanism were determined, these elements were integrated into an autonomous system which is call Needleless Self-Orienting Mechanical Actuator (N-SOMA). A diagram and photos of the N-SOMA system are shown in **Figure 4.3**. Additional design and assembly details are included in **Appendix I** and **Appendix II**.

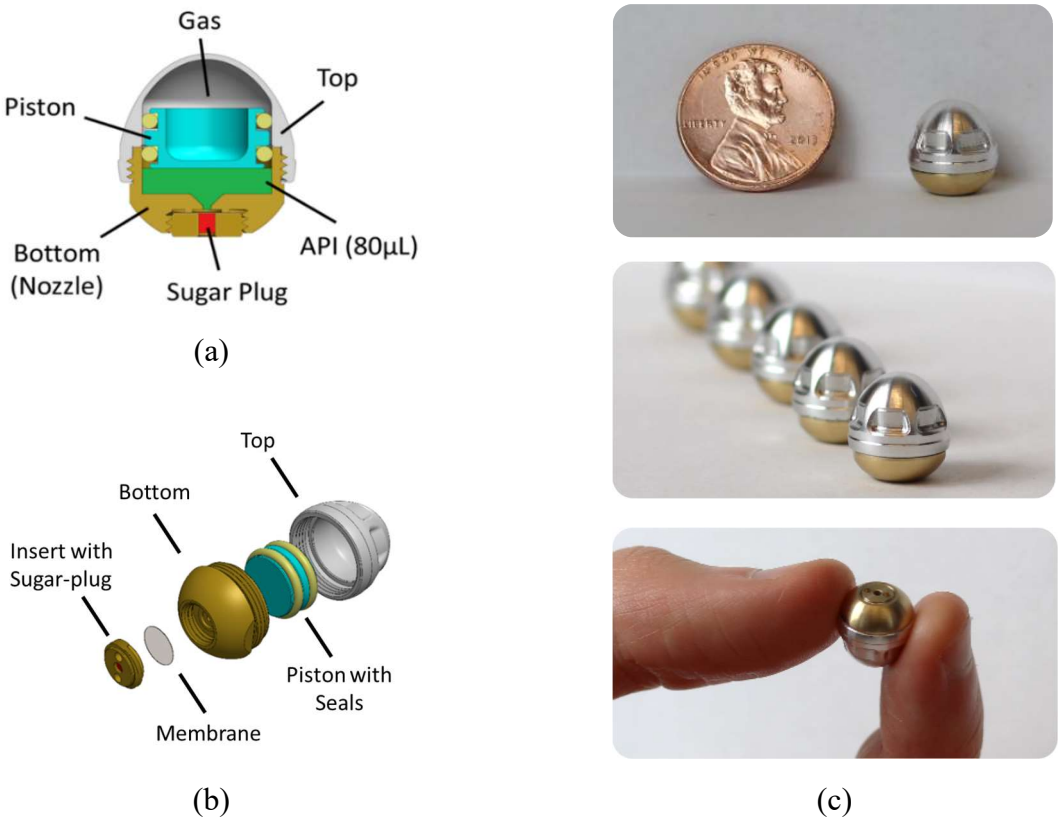


**Figure 4.3:** Graphics showing the integrated N-SOMA device. (a) Section diagram of the device; (b) Exploded view of the device (API not shown). (c) Three photos of the final device(s)

Five N-SOMA devices were produced, each weighing 2.25g when loaded. The maximum diameter of the device is 10.82mm and the maximum height 11.75mm. The API volume is 80µL – this is the largest volume that would fit within the device envelope while maintaining self-orientation properties.

It was determined that the simplest way to pressurize the device was to employ dry ice pellets. During assembly, the device is loaded with at least enough dry ice to result in saturation of the gas chamber (approx. 15mg). Excess dry ice that was loaded into the device changes to liquid-phase, while the gaseous head remains pressurized at the $CO_2$ saturation limit (64 Bar). The initial gas chamber volume is 154mm$^3$, while the final volume is 234mm$^3$. This results in a final pressure reduction to 66% of the initial pressure ($\alpha = 0.66$).

A nominal orifice diameter of 350um was selected since, according to prior tissue testing, such a diameter would produce a high delivery efficency in stomach tissue at the design pressure

of 64 Bar. However, due to a miscalculation, the actual device orifices had measured diameters of 550um. In the future, the orifice size should be corrected to ensure proper delivery characteristics.

## 4.4 Device Experiments

Tests were performed on the N-SOMA devices and subcomponents to verify that the integrated concept functioned as desired.

### 4.4.1 Triggering Tests

The triggering scheme described in **Figure 4.2** was tested 45 times total with a prototype version of the N-SOMA device . In each test, the device was pressurized to 64 Bar, submerged in deionized water, then timed until triggering was observed.

### 4.4.2 High-speed Imaging

An Edgertronic SC2 high speed camera was used to capture the triggering event and resulting jet. The frame rate used was 20000Hz. The device was placed on a plastic film, strewn across the rim of a glass beaker. This film had a 3mm diameter hole in it, on which the device orifice was centered (see **Figure 4.4**). The base of the device was then wetted with deionized water (dispensed by a pipette) and capilary action drew the water under the device causing the suger plug to dissolve. When the device triggers, the camera is manually activated and frames from three seconds prior are extracted from the camera buffer (thereby capturing the jet).

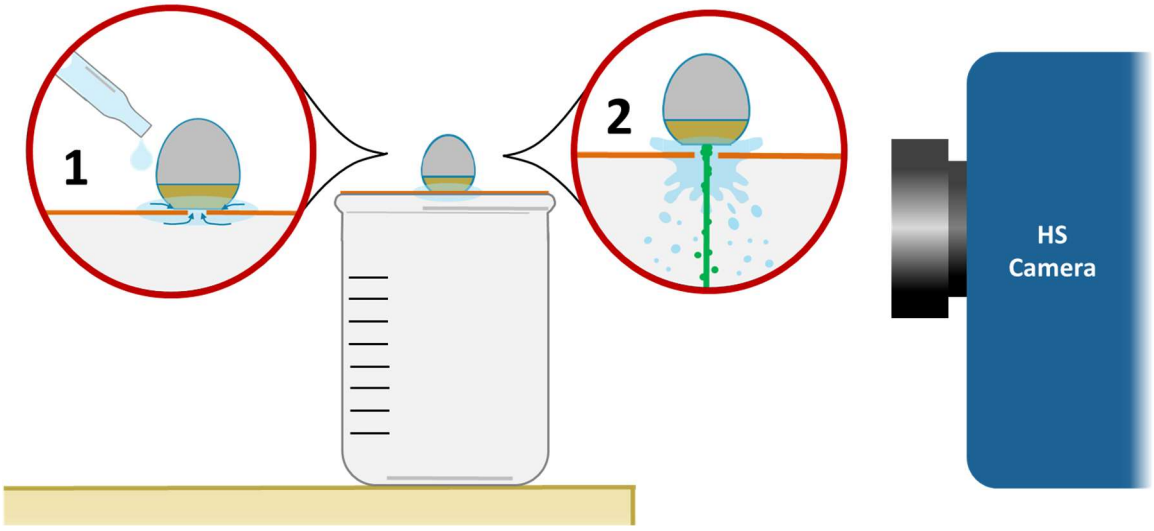


**Figure 4.4:** Test setup for high speed imaging of N-SOMA triggering

### 4.4.3 Device Tissue Performance Testing

In order to verify that the N-SOMA was able to self-orient, trigger, and deliver a jet as desired, the device was tested three times on porcine stomach tissue. Each trial consisted of loading the device with dye and pressurizing it with $CO_2$, dropping the device on stomach tissue from a distance of approximately one inch, then filming the device (with a standard digital camera) until the point of triggering. After triggering, the tissue was encapsulated in OCT gel and frozen at -80ºC within ten minutes. Tissue samples were then sectioned on a microtome/cryostat at -20ºC.

## 4.5 Device Testing Results

The measured dissolution rate for a sugar plug during triggering tests was approximately 0.25mm/min. Of the 45 triggering tests, four triggering failures were observed (91% triggering success rate). Failures occurred when the sugar-plug fractured prematurely, thus significant portions of the sugar-plug remained in front of the orifice during expulsion. Aside from premature triggering time, it was possible to identify these failures through observation of their associated membranes. Macro-lens photographs and SEM images of membranes revealed that the membrane did not rupture properly when the sugar-plug failed.

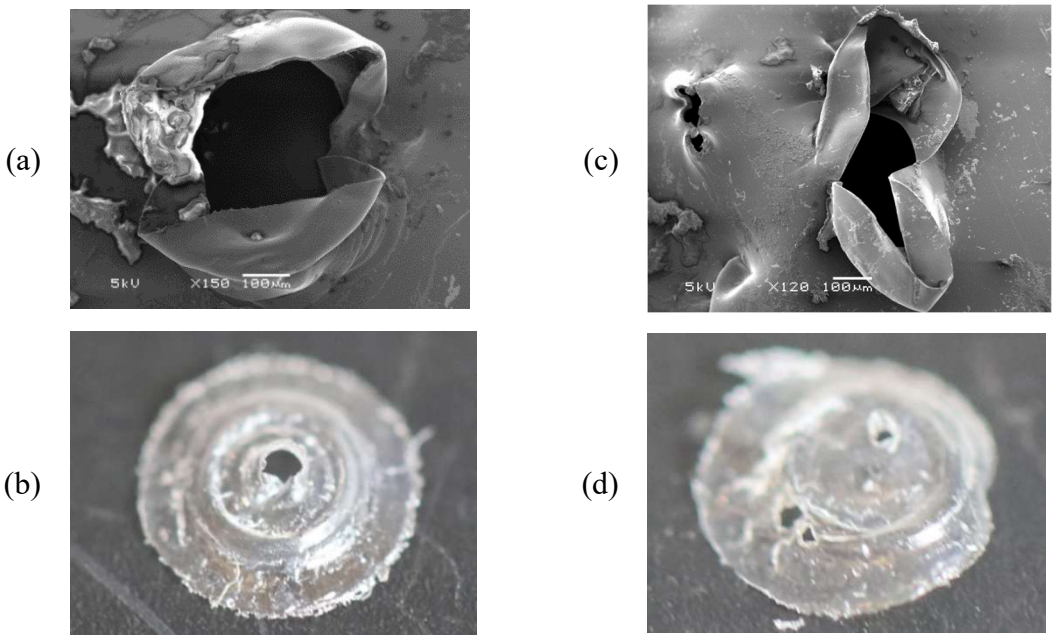


**Figure 4.5:** Images of the membrane after rupture. (a) Membrane from a successful triggering taken by SEM with 150x zoom. (b) Membrane from a successful rupture taken with a macro lens. (c) Membrane from a failed triggering taken by SEM with 120x zoom. (d) Membrane from a failed triggering taken by a DSLR camera with a macro lens

The cause of this failure is likely a result of manufacturing defects in the sugar plug such as cracks, bubbles, or imperfect crystallization (due to incomplete melting of the isomalt during potting). It is also possible that the membranes had small tears or imperfections leading to premature degradation of the isomalt by the payload fluid. Further research is necessary to understand the exact mechanism governing misfiring.

During high-speed imaging tests, triggering occurred approximately seven minutes after wetting of the device base in each trial. The high-speed data (see **Figure 4.6**) reveals three distinct regimes during jetting. First, triggering occurs and water directly underneath the device is blown forward. Then, approximately 2 ms after triggering, a columnar jet forms. After approximately 5ms, the jet cuts out, followed by a brief spray. The device continues to travel upward as a result of conservation of momentum.

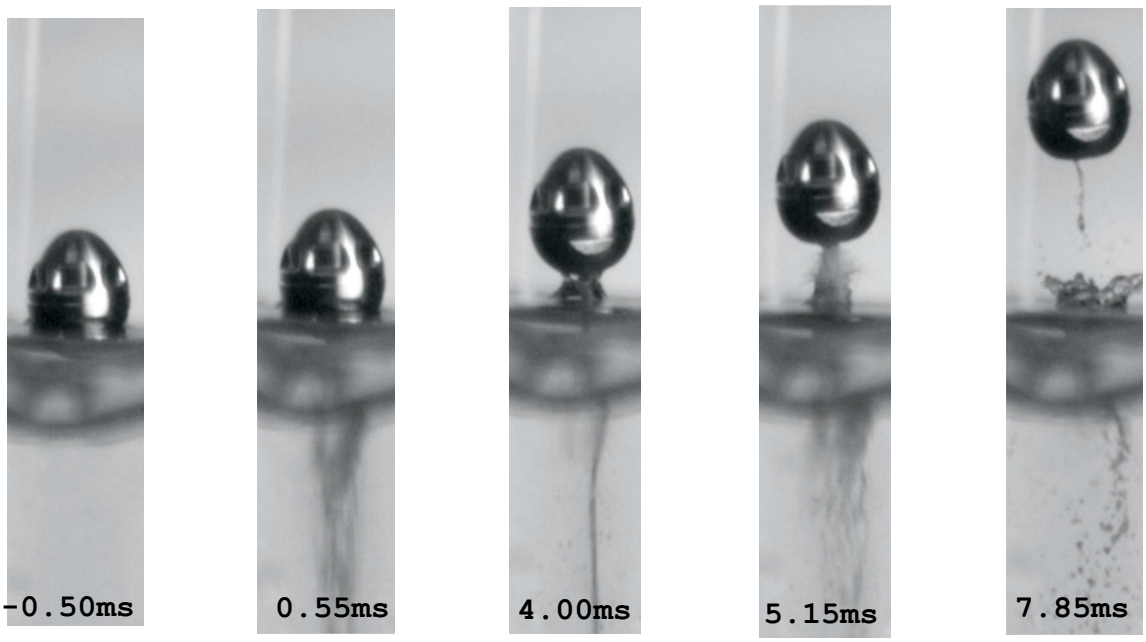


**Figure 4.6:** High-speed imaging of N-SOMA jetting event (a) prior to triggering; (b) during startup; (c) during the jetting phase; (d) after jetting ends; (e) after expulsion ends.

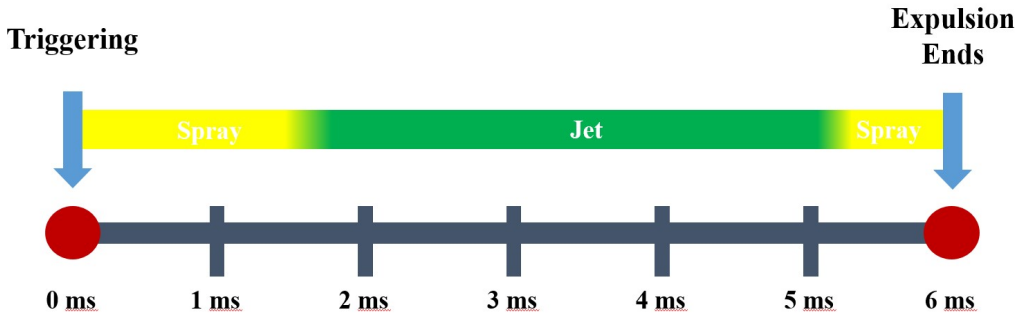


**Figure 4.7:** Timeline of the N-SOMA expulsion event

The measured jetting period shown in **Figure 4.7**—approximately 3.5ms—can be compared with the theoretical value which, according to equation (19), is 4.00ms. The discrepancies between theoretical and measured device performance can likely be attributed to the fact that the theoretical model does not include startup or shutdown transients. That said, further testing with the load sensor described in **Sub-section 2.2.2** should be carried out in order to verify the exact performance of the N-SOMA.

Of the three tissue performance tests, one trial produced a wet-shot, one a depot, and one a perforation. Triggering time was approximately 16 minutes for the wet-shot and approximately 30 minutes for the other two. Clearly, the triggering time was significantly longer on tissue than it was during high-speed testing. This can be attributed to reductions in solvent exposure during tissue testing.

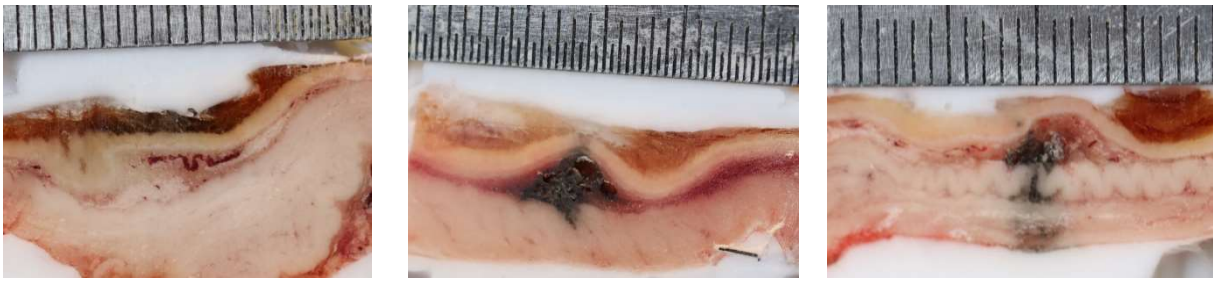

(a) (b) (c)

**Figure 4.8:** Frozen sections of stomach tissue after injection with N-SOMA. (a) Superficial "wet-shot" with no penetration. (b) depot formed in stomach tissue. (c) Perforated stomach tissue. NOTE: the largest increment on each ruler is 1mm.

Inspection of the membrane which was associated with the wet-shot confirmed that this particular membrane did not rupture properly. The relatively short triggering time of this trial also implies a defective sugar plug. This was likely the result of a manufacturing defect in the sugar-plug. As noted previously, more research is needed to further understand the source of premature firings.

Though two of the devices triggered successfully, penetration was greater than desired, resulting in perforation in one case **Figure 4.8(c),** and a depot with muscular penetration in the other **Figure 4.8(b)**. These results were expected given the prior tissue modeling and aforementioned orifice-size calculation error. Further testing of the device with a corrected orifice size should be performed before in vivo use of the device. That said, the N-SOMA device represents a promising proof-of-concept for an autonomous, ingestible jetting systems.

# 5 In Vivo Work

In vivo studies are perhaps the most important type of experiment for verifying the feasibility of any drug-delivery device. Such studies provide knowledge of pharmacokinetic profile and verify the safety of the device. This chapter details preliminary in vivo studies that were performed with jetting devices containing insulin, and bioanalytical results from said studies.

## 5.1 Experimental Methods

Each study was performed by trained veterinary technicians at MIT's animal testing facilities. Yorkshire pigs weighing between 70 and 90 kg were used. All studies were terminal studies (meaning the animal was euthanized immediately afterward). Though time constraints did not permit testing of the N-SOMA devices, it was possible to employ an early prototype of N-SOMA (without self-orientation) to generate preliminary data. This device employs the same means for power and triggering as the N-SOMA, and can store up to 40µL of fluid (**Figure 5.1**).

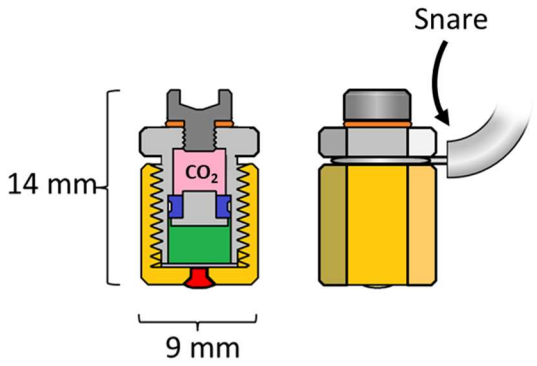


**Figure 5.1:** Surrogate tethered jetting device used for endoscopic in vivo studies

### 5.1.1 Insulin Formulation

The first step of the in-vivo procedure was to formulate aqueous insulin from solid, powder insulin. After the weight of the pig was determined, a quantity of insulin was selected to achieve a dose of 0.5 Units per kilogram (1 Unit = 0.0347 mg). The powder insulin was then added to a 0.1M NaOH solution and PF68 and HEPES were used as stabilizing agents. From there, 0.1M HCl was added to assist with dissolution of the insulin and deionized water was added if further dilution was desired. Finally, 10µL drops of NaOH were pipetted into the solution until the pH of the solution reached a value greater than or equal to 8.0 (at which point insulin is most stable). This formulation procedure was carried out the morning or evening before each in vivo study and the resulting solution was stored at 4ºC until the time of administration.

### 5.1.2 Deployment

The device was loaded with API and $CO_2$ in the operating room where the animal was sedated and intubated. The device was deployed either by direct placement into the stomach through a laparotomy, or via an over-tube with an endoscope and snare. Of the five deployments performed with this device, the first three were performed by laparotomy and the latter two by endoscope and snare. Triggering generally occurred within 15 minutes and could be identified through recoil and foaming near the base of the device. Graphics detailing deployment can be seen in **Figure 5.2**.

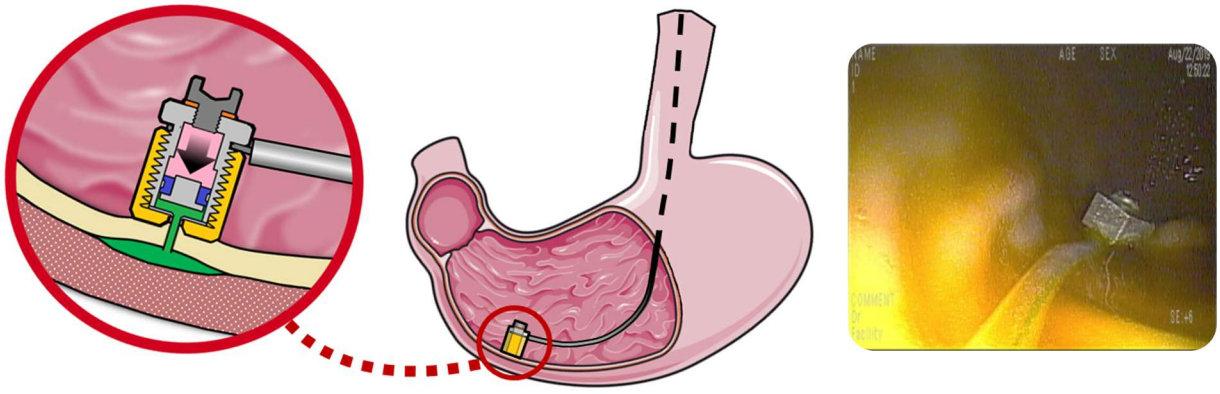

(a) (b)

**Figure 5.2:** Deployment of the surrogate tethered jetting device in a pig stomach. (a) Schematic diagram of the injection (b) Endoscopic photograph of the surrogate device being held against the stomach mucosa by a snare.

### 5.1.3 Blood Collection

Blood samples were collected by ear catheter or femoral catheter. Samples were taken in ~15minute intervals for an hour before scheduled deployment in order to ensure the stability of blood glucose levels. After deployment, blood samples were collected in five-minute intervals for the first 30 minutes, then in 15-minute intervals until two hours after deployment. Samples were stored on ice in 3mL EDTA tubes until the completion of the study.

The blood-glucose level was monitored at each draw using commercial glucose monitoring strips. If the level dropped below 20 mg/dL, an intravenous infusion of 12mL of 50% dextrose solution was administered to avoid hypoglycemia.

After completion of the study, blood samples were centrifuged at 3200rpm and plasma was extracted and stored in Eppendorf tubes. These tubes were frozen at -80°C.

## 5.2 Bioanalysis

Samples were analyzed using a custom Enzyme-linked immunosorbent assay (ELISA). This type of assay is commonly used to quantify antibodies, antigens, proteins and glycoproteins in biological samples. Of the different types of ELISA, sandwich ELISAs are the most commonly employed due to their high sensitivity [86]. As such, sandwich ELISAs were used to assess the samples collected in this study.

The sandwich ELISA procedure is divided into four steps with wash steps in between. First, a 96-well polystyrene plate is coated with capture-antibody. Next, blood plasma samples are loaded into the wells and the insulin within the samples binds to the capture-antibodies. Third, enzyme-labelled detection antibodies are added. These antibodies bind to the insulin molecules in a quantity proportional to the concentration of insulin in the sample. Finally, a substrate is added and the enzymes on the secondary antibody undergo a chromogenic reaction with this substrate. The intensity of the coloring corresponds to the concentration of insulin and can be measured directly using a plate reader.

Also, a standard curve was produced using insulin samples of known concentration to provide a calibrated reference for chromogenic measurements on each plate.

## 5.3 In Vivo Results

Three of the five device tests produced a drop in blood glucose levels and corresponding increase in blood-plasma insulin concentration. The fact that certain devices delivered insulin and others did not is likely due to manufacturing variation in device orifice size. For the prototype device, orifice sizes were observed to vary by as much as ±100µm—a problem which was addressed in later versions through use of computer numerically controlled (CNC) drilling, rather than manual drilling.

Measured insulin concentrations were variable (as seen in **Figure 5.3(b)**), likely owing to the fact that ELISAs were performed manually (rather than by an automated fluid handling system). However, the insulin concentrations trend upward during studies where significant BG drops were observed, implying that insulin was, in fact, delivered during those studies.

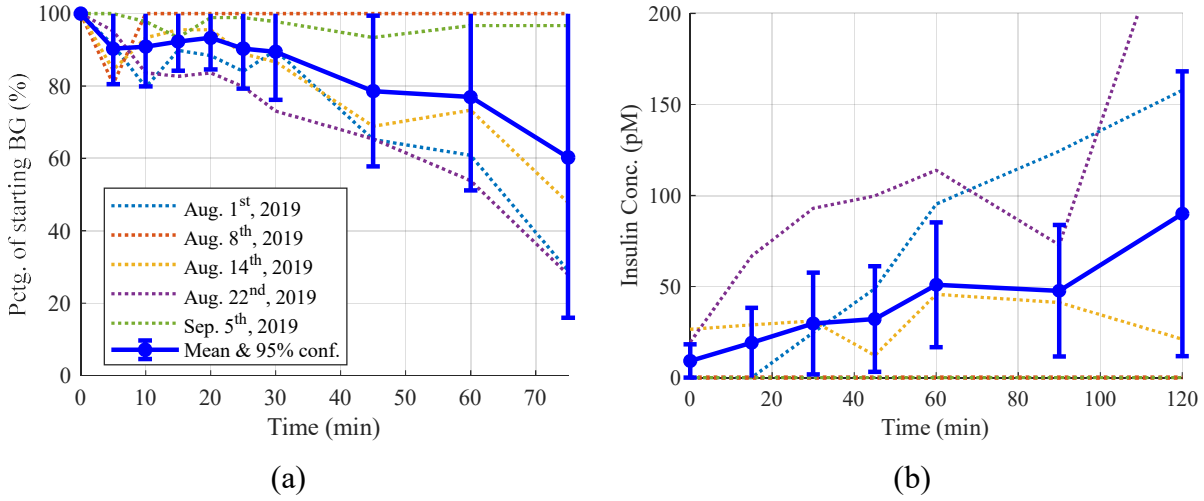


**Figure 5.3:** In vivo data from five preliminary studies with the tethered prototype device (insulin dosage 0.5 U/kg). (a) Blood glucose drop as a percentage of the starting level. (b) Blood plasma insulin concentration. NOTE: legend applies to both plots.

Though this data is preliminary, it represents a promising result, and evidence that jetting is a feasible means for the oral delivery of biologics. Future studies will employ the N-SOMA and subcutaneous controls to precisely evaluate bioavailability.

# 6 Conclusion

In this report, needleless delivery, or *jetting*, was proposed as a means for the oral delivery of biologics via penetration of mucosal tissue in the GI tract. In summary, jetting appears not only to be feasible, but potentially superior to other methods for accomplishing high bioavailability. This section briefly summarizes experimental findings, and points towards future work which will be critical in further developing ingestible jetting technology.

## 6.1 Discussion

The first experimental effort described was the development of a generalized model for compact jetting systems with sub-millimeter orifice sizes. This model considers Bernoulli energy balance and dynamic spring loading as its key components. Through empirical validation, the model was discovered to be accurate in representing the behavior of jetting systems. As such the model can be applied to predict the behavior of any jetting system at this scale, assuming nozzle efficiency and piston friction are measured beforehand.

Following the success of the above modeling effort, it was possible carry out ex vivo testing which ultimately showed that jetting was indeed a feasible means for creating submucosal depots in porcine GI tissue. These tissue experiments revealed that multiple GI tissue types require less jetting power than skin for forming depots. This data should provide the reader with a sense of design requirements for ingestible jetting systems, but should only be considered preliminary given the small number of replicates (n=1 for each point).

After discussing the experiments on jetting requirements for GI tissues, the thesis detailed implementation of a mm-scale “proof-of-concept” device that is able to autonomously localize and

trigger a jetting delivery event. The functionality of the device was verified with high-speed imaging, and the device was tested on tissue with promising results. In the process of developing this device, an isomalt-based triggering mechanism was developed. This dissolvable triggering mechanism is capable of retaining high pressures and can be designed to trigger at a specific time based on its length. Occasional failures of the triggering mechanism were observed (9% failure-rate). These failures will be addressed in future work.

Lastly, preliminary in vivo data was reported showing delivery of insulin via prototype versions of the autonomous device. In these experiments, blood glucose drops exceeding 80% were observed prior to intravenous infusion of dextrose to restore normal levels. Three of five deliveries were successful, likely due to the fact that devices had varying orifice sizes. Thus, similarly to the ex vivo data, the reader should only consider the in vivo data as preliminary. Having said that, the reported work hints at high bioavailability, further substantiating the claim that jets have a large potential to make an impact in the field of oral delivery of macromolecules.

## 6.2 Future Work

Much remains to be done with regards to characterizing jetting prior to its translation into a clinical setting. In this section, future activities that will be critical in proving the success of ingestible jetting technology will be discussed.

With regards to jetting mechanistic modeling, neither viscous friction losses nor aerodynamic losses were considered. Such inputs could prove useful in modeling the jetting behavior of drug formulations with viscosity higher than water (e.g. insulin), and evaluating the impact of standoff distance between the jet and target surface. Furthermore, computational flow simulations could be implemented to model nozzle losses, which are currently determined empirically.

For tissue characterization, it will be important to add many more replicates to the current data set in order to improve the fidelity of the reported power requirements for each tissue type. Furthermore, switching contrast agents from the current barium-sulfate suspension, to an iodine based solution will provide potential improvements in micro-CT data quality. As well, future work should include small intestine studies, and work which characterizes the impact of variation of jetting incidence angle on delivery efficiency,

Aside from additional empirical tissue testing, it may be worth investigating a numerical model for the penetration of GI tissue by jets. Little is currently understood about the formation of a fluid depot between layers of GI tissue. To achieve a model that can predict formation of these structures, it may be necessary to combine elements of penetrator mechanics, nonlinear soft-tissue mechanics, diffusion mechanics, as well as empirical data.

Also yet to be understood are certain safety implications of deploying a jetting device in the GI tract. Tissue trauma resulting in scarring or infection, for example, could obviate certain practical uses of this technology such as daily dosing. Furthermore, it was observed that there was a significant content of air bubbles in many ex vivo depots—a phenomenon that is not well understood and which could have future safety implications. As such, studies to address the above safety concerns should be performed as soon as possible. Examples of methods could include daily deployment of jetting devices in a large animal along with regular endoscopic inspection of the GI tract; and terminal studies, where tissue from an injection site is excised, sectioned and stained for inflammatory response markers.

With regards to device development, additional improvements to the sugar-plug should be investigated with the goal of increasing success rate. Implementation of a standardized fabrication procedure for the sugar-plugs and stringent inspection procedures could be useful to that end. Also, different autonomous device concepts utilizing alternative power sources, triggering mechanisms, localization techniques, and target organs should be investigated.

Lastly, generation of more robust pharmacokinetic data will be essential in evaluating the virtual bioavailability of jetting devices. These studies should include control trials, investigation of multiple therapeutics, and evaluation of the impact of dosing frequency and volume.

# Bibliography


[1] J. Mantaj and D. Vlasaliu, “Recent advances in the oral delivery of biologics,” *Pharm. J.*, Jan. 2020.

[2] S. Yougbare *et al.*, “Antimicrobial gold nanoclusters: Recent developments and future perspectives,” *International Journal of Molecular Sciences*, vol. 20, no. 12. MDPI AG, p. 2924, 02-Jun-2019.

[3] S. Maiti, “Nanometric Biopolymer Devices for Oral Delivery of Macromolecules with Clinical Significance,” in *Multifunctional Systems for Combined Delivery, Biosensing and Diagnostics*, Elsevier, 2017, pp. 109–138.

[4] T. Uhlig *et al.*, “The emergence of peptides in the pharmaceutical business: From exploration to exploitation,” *EuPA Open Proteomics*, vol. 4, pp. 58–69, May 2014.

[5] M. Aitken, “Global Medicines Use in 2020: Outlook and Implications,” Nov. 2015.

[6] “Biologics Market Size, Share 2020|Global Industry Analysis and Forecast (2020-2023) by Growth, Application and Region - GuruFocus.com.” [Online]. Available: https://www.gurufocus.com/news/1035283/biologics-market-size-share-2020global-industry-analysis-and-forecast-20202023-by-growth-application-and-region. [Accessed: 13-May-2020].

[7] “U.S. Diabetes Surveillance System.” [Online]. Available: https://gis.cdc.gov/grasp/diabetes/diabetesatlas.html. [Accessed: 13-May-2020].

[8] World Health Organization, “ADHERENCE TO LONG-TERM THERAPIES: Evidence for action,” 2003.

[9] W. H. Polonsky and R. R. Henry, “Poor medication adherence in type 2 diabetes: Recognizing the scope of the problem and its key contributors,” *Patient Preference and Adherence*, vol. 10. Dove Medical Press Ltd., pp. 1299–1306, 22-Jul-2016.

[10] G. B. Sarbacker and E. M. Urteaga, “Adherence to insulin therapy,” *Diabetes Spectr.*, vol. 29, no. 3, pp. 166–170, Aug. 2016.

[11] T. A. S. Aguirre, D. Teijeiro-Osorio, M. Rosa, I. S. Coulter, M. J. Alonso, and D. J. Brayden, “Current status of selected oral peptide technologies in advanced preclinical development and in clinical trials,” *Advanced Drug Delivery Reviews*, vol. 106. Elsevier B.V., pp. 223–241, 15-Nov-2016.

[12] D. Herkert *et al.*, “Cost-Related Insulin Underuse Among Patients With Diabetes,” *JAMA Internal Medicine*, vol. 179, no. 1. American Medical Association, pp. 112–114, 01-Jan-2019.

[13] E. Buysman, C. Conner, M. Aagren, J. Bouchard, and F. Liu, “Adherence and persistence to a regimen of basal insulin in a pre-filled pen compared to vial/syringe in insulin-naïve patients with type 2 diabetes,” 2011.

[14] T. Weinhold, M. Del Zotto, J. Rochat, J. Schiro, S. Pelayo, and R. Marcilly, “Improving the safety of disposable auto-injection devices: a systematic review of use errors,” *AAPS Open*, vol. 4, no. 1, pp. 1–14, Dec. 2018.

[15] J. Guérin, “Gazette Médicale de Paris,” 1866. [Online]. Available: https://books.google.com/books?id=X3ZEAAAAcAAJ&printsec=frontcover#v=onepage&q&f=false. [Accessed: 14-May-2020].

[16] “Becton-Dickinson & Co. v. Robert P. Scherer Corp., 106 F. Supp. 665 (E.D. Mich. 1952),” *Justia*, 1952. [Online]. Available: https://law.justia.com/cases/federal/district-courts/FSupp/106/665/1649380/. [Accessed: 14-May-2020].

[17] N. Snelling, “The history of the hypodermic needle,” *Live Better*, 2014. [Online]. Available: https://www.medibank.com.au/livebetter/be-magazine/wellbeing/the-history-of-the-hypodermic-needle/. [Accessed: 14-May-2020].

[18] J. O. Eastland, “Study of the Subcommittee on Patents, Trademarks, and Copyrights of the Committtee on the Judiciary United States Senate, Eighty-sixth Congress, Second Session, Pursuant to S. Res. 240, Study No. 28,” *U.S. Government Printing Office*, 1981. [Online]. Available: https://books.google.com/books?id=Ely_jBbvZuMC&pg=RA5-PP7&lpg=RA5-PP7&dq=3)+Government+Assistance+to+Invention+and+Research:+A+Legislative+History,+page+10&source=bl&ots=oCwvU7myXJ&sig=ACfU3U14MvrVVfE0UUb4DW8ltFOywwFqMQ&hl=en&sa=X&ved=2ahUKEwjunf_j3LPpAhU. [Accessed: 14-May-2020].

[19] “Google Patents: advanced search on classification A61M5/30 - Syringes for injection by jet action, without needle, e.g. for use with replaceable ampoules or carpules,” 2020. .

[20] “Syringe Needle Gauge Chart | Sigma-Aldrich.” [Online]. Available: https://www.sigmaaldrich.com/chemistry/stockroom-reagents/learning-center/technical-library/needle-

gauge-chart.html. [Accessed: 14-May-2020].
[21] O. A. Shergold, N. A. Fleck, and T. S. King, “The penetration of a soft solid by a liquid jet, with application to the administration of a needle-free injection,” *J. Biomech.*, vol. 39, no. 14, pp. 2593–2602, Jan. 2006.
[22] K. Aran *et al.*, “An oral microjet vaccination system elicits antibody production in rabbits,” *Sci. Transl. Med.*, vol. 9, no. 380, p. eaaf6413, Mar. 2017.
[23] “Technology – Baywind Bioventures.” [Online]. Available: http://baywindbio.com/jetcap/. [Accessed: 26-May-2020].
[24] T. D. Brown, K. A. Whitehead, and S. Mitragotri, “Materials for oral delivery of proteins and peptides,” *Nature Reviews Materials*, vol. 5, no. 2. Nature Research, pp. 127–148, 01-Feb-2020.
[25] “CAPSULE DEVICE FOR DELIVERY OF ACTIVE AGENT TO GASTROINTESTINAL TRACT: WO2020041774 (A1) — 2020-02-27,” *Espacenet*, 2020. [Online]. Available: https://worldwide.espacenet.com/publicationDetails/description?CC=WO&NR=2020041774A1&KC=A1&FT=D&ND=3&date=20200227&DB=&locale=en_EP. [Accessed: 26-May-2020].
[26] “ELECTROMECHANICAL INGESTIBLE DEVICE FOR DELIVERY OF A DISPENSABLE SUBSTANCE: WO2018049133 (A1) — 2018-03-15,” *Espacenet*, 2018. [Online]. Available: https://worldwide.espacenet.com/publicationDetails/description?CC=WO&NR=2018049133A1&KC=A1&FT=D&ND=&date=20180315&DB=&locale=en_EP. [Accessed: 26-May-2020].
[27] A. Abramson *et al.*, “An ingestible self-orienting system for oral delivery of macromolecules,” *Science (80-. ).*, vol. 363, no. 6427, pp. 611–615, Feb. 2019.
[28] A. Abramson *et al.*, “A luminal unfolding microneedle injector for oral delivery of macromolecules,” *Nat. Med.*, vol. 25, no. 10, pp. 1512–1518, Oct. 2019.
[29] “Home - Rani Therapeutics.” [Online]. Available: https://www.ranitherapeutics.com/. [Accessed: 13-May-2020].
[30] “US10478396B2 - Therapeutic agent preparations for delivery into a lumen of the intestinal tract using a swallowable drug delivery device - Google Patents.” [Online]. Available: https://patents.google.com/patent/US10478396B2/en?assignee=rani+therapeutics&oq=rani+therapeutics. [Accessed: 13-May-2020].
[31] J. Y. Sung *et al.*, “Systemic absorption of epinephrine after endoscopic submucosal injection in patients with bleeding peptic ulcers,” *Gastrointest. Endosc.*, vol. 39, no. 1, pp. 20–22, 1993.
[32] B. J. Aungst, “Absorption enhancers: Applications and advances,” *AAPS Journal*, vol. 14, no. 1. Springer, pp. 10–18, 22-Mar-2012.
[33] S. T. Buckley *et al.*, “Transcellular stomach absorption of a derivatized glucagon-like peptide-1 receptor agonist,” *Sci. Transl. Med.*, vol. 10, no. 468, Nov. 2018.
[34] R. Singh and J. W. Lillard, “Nanoparticle-based targeted drug delivery,” *Experimental and Molecular Pathology*, vol. 86, no. 3. NIH Public Access, pp. 215–223, Jun-2009.
[35] W. H. De Jong and P. J. A. Borm, “Drug delivery and nanoparticles: Applications and hazards,” *International Journal of Nanomedicine*, vol. 3, no. 2. Dove Press, pp. 133–149, 2008.
[36] “EU public health report on Nanotechnologies,” 2010. [Online]. Available: https://ec.europa.eu/health/scientific_committees/opinions_layman/en/nanotechnologies/l-3/6-health-effects-nanoparticles.htm#2p0. [Accessed: 13-May-2020].
[37] E. J. Bunggulawa *et al.*, “Recent advancements in the use of exosomes as drug delivery systems 06 Biological Sciences 0601 Biochemistry and Cell Biology,” *Journal of Nanobiotechnology*, vol. 16, no. 1. BioMed Central Ltd., p. 81, 16-Oct-2018.
[38] D. Ha, N. Yang, and V. Nadithe, “Exosomes as therapeutic drug carriers and delivery vehicles across biological membranes: current perspectives and future challenges,” *Acta Pharmaceutica Sinica B*, vol. 6, no. 4. Chinese Academy of Medical Sciences, pp. 287–296, 01-Jul-2016.
[39] “Iontophoresis - an overview | ScienceDirect Topics.” [Online]. Available: https://www.sciencedirect.com/topics/agricultural-and-biological-sciences/iontophoresis. [Accessed: 13-May-2020].
[40] C. Gao *et al.*, “A directly swallowable and ingestible micro-supercapacitor,” *J. Mater. Chem. A*, vol. 8, no. 7, pp. 4055–4061, Feb. 2020.
[41] A. Wanasathop and S. Kevin Li, “Iontophoretic drug delivery in the oral cavity,” *Pharmaceutics*, vol. 10, no. 3. MDPI AG, 01-Sep-2018.
[42] “First use of insulin in treatment of diabetes on this day in 1922 | Diabetes UK.” [Online]. Available: https://www.diabetes.org.uk/about_us/news_landing_page/first-use-of-insulin-in-treatment-of-diabetes-88-years-ago-today. [Accessed: 13-May-2020].

[43] S. L. Aronoff, K. Berkowitz, B. Shreiner, and L. Want, “Glucose Metabolism and Regulation: Beyond Insulin and Glucagon,” *Diabetes Spectr.*, vol. 17, no. 3, pp. 183–190, Jul. 2004.
[44] J. J. Holst, “The physiology of glucagon-like peptide 1,” *Physiological Reviews*, vol. 87, no. 4. pp. 1409–1439, Oct-2007.
[45] M. Shah and A. Vella, “Effects of GLP-1 on appetite and weight,” *Reviews in Endocrine and Metabolic Disorders*, vol. 15, no. 3. Kluwer Academic Publishers, pp. 181–187, 2014.
[46] J. E. Vela Ramirez, L. A. Sharpe, and N. A. Peppas, “Current state and challenges in developing oral vaccines,” *Advanced Drug Delivery Reviews*, vol. 114. Elsevier B.V., pp. 116–131, 15-May-2017.
[47] “Monoclonal antibody drugs for cancer: How they work - Mayo Clinic.” [Online]. Available: https://www.mayoclinic.org/diseases-conditions/cancer/in-depth/monoclonal-antibody/art-20047808. [Accessed: 14-May-2020].
[48] S. Singh *et al.*, “Monoclonal Antibodies: A Review,” *Curr. Clin. Pharmacol.*, vol. 13, no. 2, pp. 85–99, Oct. 2018.
[49] “Monoclonal Antibodies: List, Types, Side Effects, FDA Uses (Cancer).” [Online]. Available: https://www.medicinenet.com/monoclonal_antibodies/article.htm#what_are_the_uses_for_monoclonal_antibodies. [Accessed: 14-May-2020].
[50] M. Terry, “Report: Projected Sales of 10 Top-Selling Drugs Through 2024 | BioSpace,” 2019. [Online]. Available: https://www.biospace.com/article/top-10-drug-sales-projected-through-2024/. [Accessed: 14-May-2020].
[51] G. C. Williams and P. J. Sinko, “Oral absorption of the HIV protease inhibitors: A current update,” *Adv. Drug Deliv. Rev.*, vol. 39, no. 1–3, pp. 211–238, Oct. 1999.
[52] Y. He, D. N. Xia, Q. X. Li, J. S. Tao, Y. Gan, and C. Wang, “Enhancement of cellular uptake, transport and oral absorption of protease inhibitor saquinavir by nanocrystal formulation,” *Acta Pharmacol. Sin.*, vol. 36, no. 9, pp. 1151–1160, Sep. 2015.
[53] “Hormonal therapy - Canadian Cancer Society.” [Online]. Available: https://www.cancer.ca/en/cancer-information/diagnosis-and-treatment/chemotherapy-and-other-drug-therapies/hormonal-therapy/?region=on. [Accessed: 14-May-2020].
[54] L. R. Newson, “Best practice for HRT: Unpicking the evidence,” *British Journal of General Practice*, vol. 66, no. 653. Royal College of General Practitioners, pp. 597–598, 01-Dec-2016.
[55] W. Moote and H. Kim, “Allergen-specific immunotherapy,” *Allergy, Asthma Clin. Immunol.*, vol. 7, no. S1, p. S5, Dec. 2011.
[56] “Allergenic Extracts, Pollen more - FDA prescribing information, side effects and uses.” [Online]. Available: https://www.drugs.com/pro/allergenic-extracts-pollen-more.html. [Accessed: 14-May-2020].
[57] H. J. Dworken, W. T. Keeton, N. Carr Hightower, and W. Sircus, “Human digestive system | Britannica,” *Encyclopedia Britannica*. [Online]. Available: https://www.britannica.com/science/human-digestive-system/Esophagus. [Accessed: 14-May-2020].
[58] B. Kuo and D. Urma, “Esophagus - anatomy and development : GI Motility online Esophagus - anatomy and development Esophagus - anatomy and development : GI Motility online,” *Rev. Lit. Arts Am.*, pp. 1–26, May 2008.
[59] “The esophagus - Canadian Cancer Society.” [Online]. Available: https://www.cancer.ca/en/cancer-information/cancer-type/esophageal/esophageal-cancer/the-esophagus/?region=on. [Accessed: 14-May-2020].
[60] M. J. Ferrua and R. P. Singh, “Understanding the fluid dynamics of gastric digestion using computational modeling,” *Procedia Food Sci.*, vol. 1, pp. 1465–1472, 2011.
[61] A. H. Maurer, “Gastrointestinal motility, part 1: Esophageal Transit and Gastric Emptying,” *J. Nucl. Med. Technol.*, vol. 44, no. 1, pp. 1–11, Aug. 2016.
[62] L. T. Weaver, S. Austin, and T. J. Cole, “Small intestinal length: A factor essential for gut adaptation,” *Gut*, vol. 32, no. 11, pp. 1321–1323, 1991.
[63] C. G. Cronin, E. Delappe, D. G. Lohan, C. Roche, and J. M. Murphy, “Normal small bowel wall characteristics on MR enterography,” *Eur. J. Radiol.*, vol. 75, no. 2, pp. 207–211, Aug. 2010.
[64] A. L. Mescher, “Junqueira’s Basic Histology,” *McGraw-Hill*, 2016. [Online]. Available: http://histonano.com/books/Junqueira’s Basic Histology PDF WHOLE BOOK/15. Digestive Tract.htm. [Accessed: 14-May-2020].
[65] S. N. Rasmussen and P. Riis, “Rectal wall thickness measured by ultrasound in chronic inflammatory diseases of the colon,” *Scand. J. Gastroenterol.*, vol. 20, no. 1, pp. 109–114, 1985.
[66] T. Fernandes, M. I. Oliveira, R. Castro, B. Araújo, B. Viamonte, and R. Cunha, “Bowel wall thickening at

CT: Simplifying the diagnosis," *Insights into Imaging*, vol. 5, no. 2. Springer Berlin, pp. 195–208, 2014.
[67] "Molecular Expressions Microscopy Primer: Specialized Microscopy Techniques - Differential Interference Contrast Image Gallery - Human Cheek Epithelial Cells." [Online]. Available: https://micro.magnet.fsu.edu/primer/techniques/dic/dicgallery/cheekcellssmall.html. [Accessed: 14-May-2020].
[68] Z. Angelo and C. Polyvios, "Alternative practices of achieving anaesthesia for dental procedures: a review," *J. Dent. Anesth. Pain Med.*, vol. 18, no. 2, p. 79, 2018.
[69] P. Haggard and L. de Boer, "Oral somatosensory awareness," *Neuroscience and Biobehavioral Reviews*, vol. 47. Elsevier Ltd, pp. 469–484, 01-Nov-2014.
[70] OpenStax, "Open Text British Columbia: 157 23.4 The Stomach." OpenStax, 06-Mar-2013.
[71] V. Mahadevan, "Anatomy of the small intestine," *Surgery (United Kingdom)*, vol. 35, no. 8. Elsevier Ltd, pp. 407–412, 01-Aug-2017.
[72] L. L. Azzouz and S. Sharma, *Physiology, Large Intestine*. StatPearls Publishing, 2018.
[73] A. Karunaharamoorthy, "Rectum: Anatomy, histology, function," *kenhub.com*, 2020. [Online]. Available: https://www.kenhub.com/en/library/anatomy/the-rectum. [Accessed: 14-May-2020].
[74] S. Mitragotri, "Current status and future prospects of needle-free liquid jet injectors," *Nat. Rev. Drug Discov.*, vol. 5, no. 7, pp. 543–548, Jul. 2006.
[75] J. Schramm-Baxter and S. Mitragotri, "Needle-free jet injections: dependence of jet penetration and dispersion in the skin on jet power," *J. Control. Release*, vol. 97, no. 3, pp. 527–535, Jul. 2004.
[76] J. Schramm and S. Mitragotri, "Transdermal Drug Delivery by Jet Injectors: Energetics of Jet Formation and Penetration," 2002.
[77] "Rocket Thrust Equations." [Online]. Available: https://www.grc.nasa.gov/WWW/K-12/rocket/rktthsum.html. [Accessed: 14-May-2020].
[78] "Parker Hannifin Snap-Tite BPHC-8 Quick Disconnect Female Hot Water 1/2" Brass Fitting." [Online]. Available: https://www.americandivingsupply.com/BPHC-8-QD-Female-Hot-Water-1-2-Brass-Fitting-p/bphc-8.htm. [Accessed: 14-May-2020].
[79] D. M. Bass, M. Prevo, and D. S. Waxman, "Gastrointestinal safety of an extended-release, nondeformable, oral dosage form (OROS®): A retrospective study," *Drug Saf.*, vol. 25, no. 14, pp. 1021–1033, 2002.
[80] L. MacKenzie-Smith, P. Marchi, H. Thorne, S. Timeus, R. Young, and P. Le Calvé, "Patient Preference and Physician Perceptions of Patient Preference for Oral Pharmaceutical Formulations: Results from a Real-Life Survey," *Inflamm. Intest. Dis.*, vol. 3, no. 1, pp. 43–51, 2018.
[81] K. Klotz, W. Weistenhöfer, F. Neff, A. Hartwig, C. Van Thriel, and H. Drexler, "The health effects of aluminum exposure," *Dtsch. Arztebl. Int.*, vol. 114, no. 39, pp. 653–659, Sep. 2017.
[82] C. J. Bettinger, "Materials Advances for Next-Generation Ingestible Electronic Medical Devices," *Trends Biotechnol.*, vol. 33, no. 10, pp. 575–585, Oct. 2015.
[83] F. Cervero, "10 Neurophysiology of gastrointestinal pain," *Baillieres. Clin. Gastroenterol.*, vol. 2, no. 1, pp. 183–199, 1988.
[84] "Portal Instruments." [Online]. Available: https://www.portalinstruments.com/. [Accessed: 14-May-2020].
[85] Z. Li *et al.*, "Exceptional supercapacitor performance from optimized oxidation of graphene-oxide," *Energy Storage Mater.*, vol. 17, pp. 12–21, Feb. 2019.
[86] "Overview of ELISA | Thermo Fisher Scientific - US." [Online]. Available: https://www.thermofisher.com/us/en/home/life-science/protein-biology/protein-biology-learning-center/protein-biology-resource-library/pierce-protein-methods/overview-elisa.html. [Accessed: 14-May-2020].

# Appendices

## I. Additional N-SOMA Device Design Details

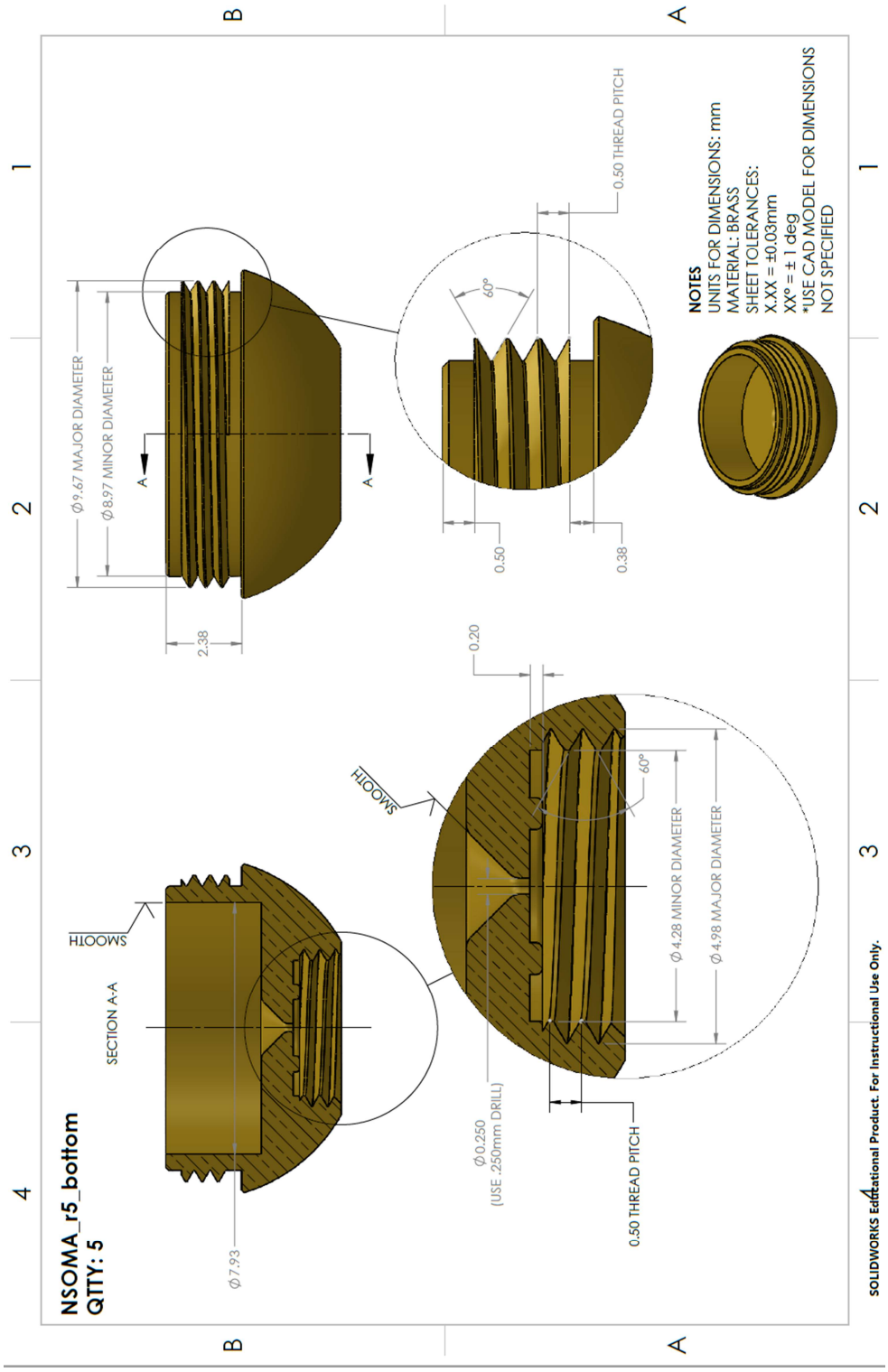

**NSOMA_r5_top**
**QTTY: 5**

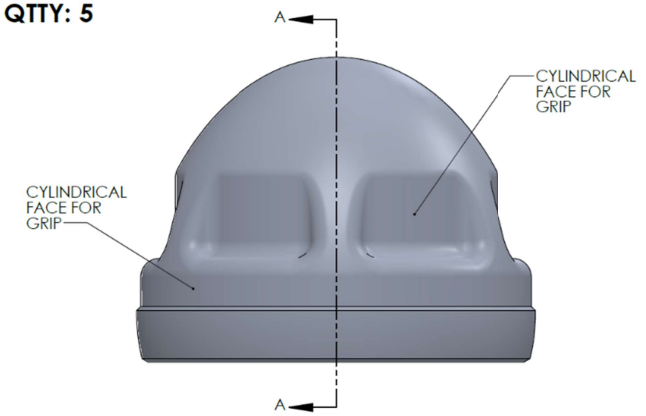


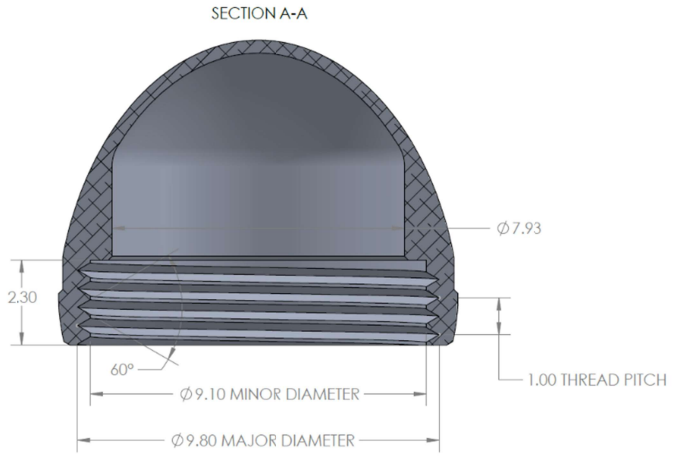


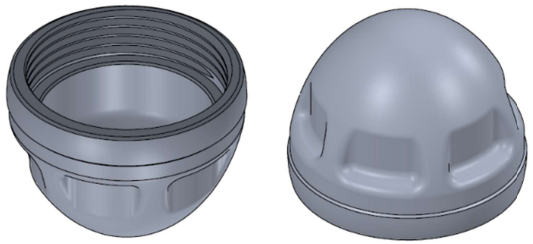

**NOTES**
UNITS FOR DIMENSIONS: mm
MATERIAL: 7075 ALUMINUM
SHEET TOLERANCES:
X.XX = ±0.03mm
XX° = ± 1 deg
*USE CAD MODEL FOR DIMENSIONS NOT SPECIFIED

**NSOMA_r5_piston**
**QTTY: 5**

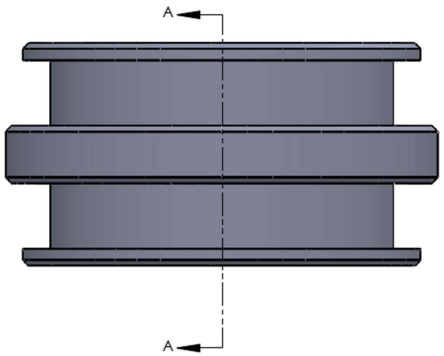


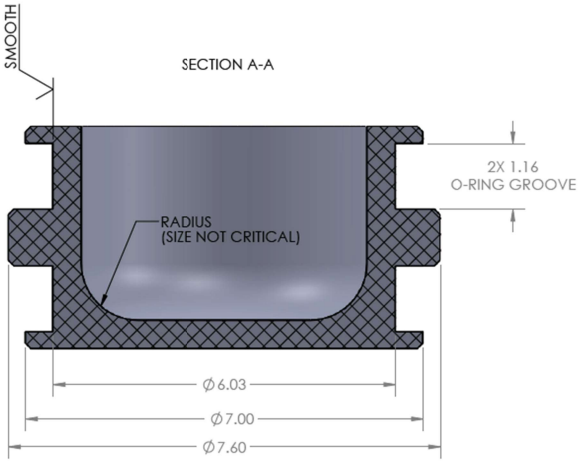


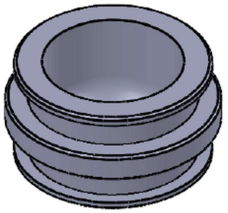

**NOTES**
UNITS FOR DIMENSIONS: mm
MATERIAL: POM (DELRIN)
SHEET TOLERANCES:
X.XX = ±0.03mm
*USE CAD MODEL FOR DIMENSIONS NOT SPECIFIED

# NSOMA_r5_screw_plug
**QTTY: 5**

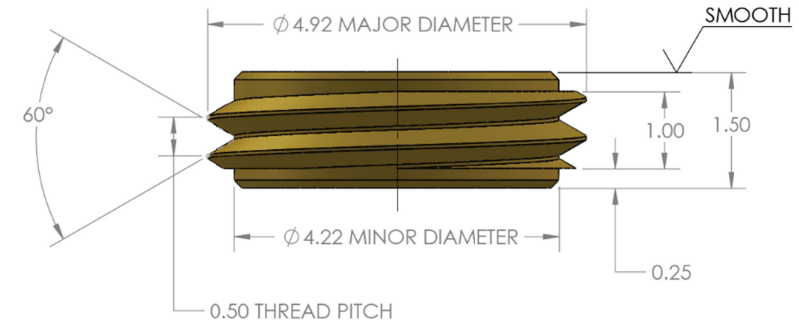


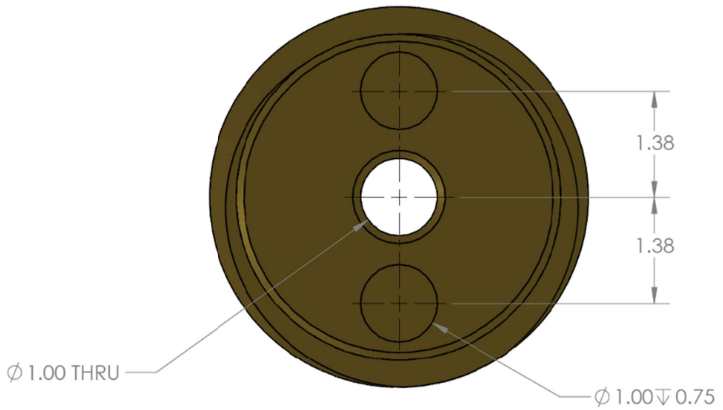


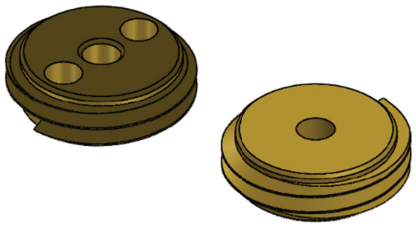

**NOTES**
UNITS FOR DIMENSIONS: mm
MATERIAL: BRASS
SHEET TOLERANCES:
X.XX = ±0.03mm
XX° = ± 1 deg
*USE CAD MODEL FOR DIMENSIONS NOT SPECIFIED

## II. N-SOMA Device Assembly Procedure

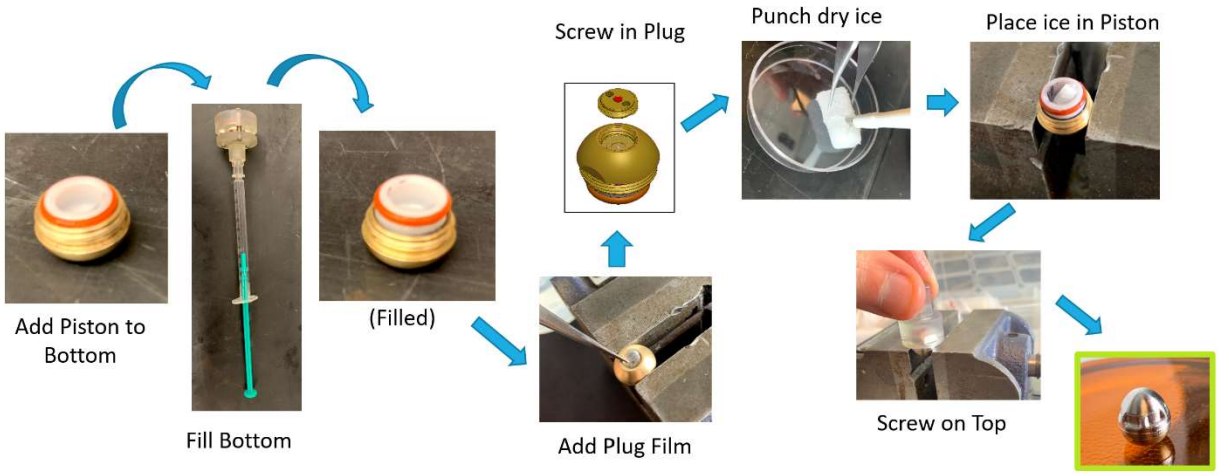


## III. N-SOMA Device Leakage Testing

- Devices were filled with $CO_2$ then weighed over time
- Average leak rate = 0.1mg/min
- Projected average endurance = 14hr (more than sufficient to deploy in-vivo)
- Variation likely due to tolerances in device parts (specifically, Top and Piston)
- Improved sealing would require metallization of seals

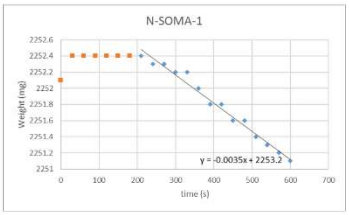


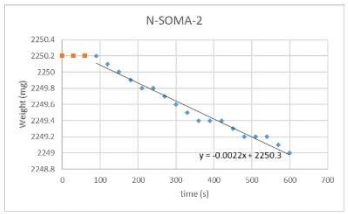


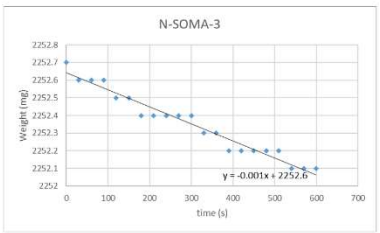


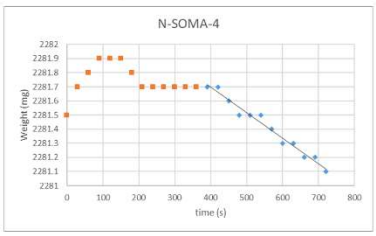


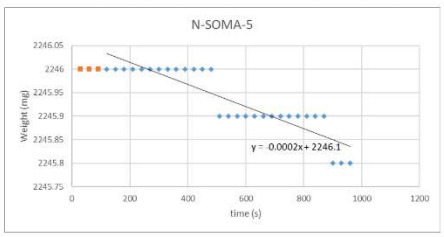

## IV. MATLAB Implementation of Mechanistic Model

```
clear all;
close all;

%Inputs
F_s = 150; %Initial force (N)
d_j = [150 200 250 300 350].*10^-6; %Nozzle diameter (m)
alpha = 0.45; %Final spring force as fraction of initial

%Force Curve
figure; hold on; grid on;
    set(gca, 'FontName', 'Times New Roman')
    colors = {'r', 'b', 'g', 'c', 'k'};
    for i = 1:length(d_j)
        [t, v, F, P] = gen_profile(F_s, d_j(i), alpha);
        plot(t,F, colors{i}, 'LineWidth', 1.5)
    end
    xlabel('Time (s)')
    ylabel('Jet Force (N)')
    legend('150\mum','200\mum','250\mum','300\mum','350\mum');
    title('Jetting Force')

%Power Curve
figure; hold on; grid on;
    set(gca, 'FontName', 'Times New Roman')
    colors = {'r', 'b', 'g', 'c', 'k'};
    for i = 1:length(d_j)
        [t, v, F, P] = gen_profile(F_s, d_j(i), alpha);
        plot(t,P, colors{i}, 'LineWidth', 1.5)
    end
    xlabel('Time (s)')
    ylabel('Jet Power (W)')
    legend('150\mum','200\mum','250\mum','300\mum','350\mum');
    title('Jetting Power')


function [t, v, F, P] = gen_profile(F_s, d_n, alpha)

    %Fixed Parameters
    L = 7*10^-3; %stroke (m)
    rho = 1000; %density (kg/m^3)
    d_p = 6*10^-3; %Ampule diameter (m)
    F_f = 4; %Friction losses (N)
    Eff_nozz = 0.80; %Nozzle Efficiency

    %Area Calcs
    A_p = pi*d_p^2/4;
    A_j = pi*d_n^2/4;

    %Energy input
    k = F_s*(1-alpha)/L;
    E_in = 1/2*L*F_s*(alpha+1);

    %Accounting for friction losses in the piston
    F_s1 = F_s-F_f;
    Eff_fric = 1-2*F_f/(F_s*(alpha+1));

    %Constant for simplifying differential equation (with efficiency loss)
    C2 = 1/2*rho*1/Eff_nozz*A_p^3/A_j^2;

    %Define time vector
    t_step = .000001;
    t_max = 2/k*(sqrt(C2*F_s1)-sqrt(C2*(F_s1-k*L)));
    t_vec = 0:t_step:t_max;

    %Piston dynamics
    x_p = t_vec*sqrt(F_s1/C2)-k*(t_vec).^2/(4*C2);
    v_p = sqrt(F_s1/C2)-k*t_vec/(2*C2);
```

```
    %Calculate Jetting Performance
    v_j = A_p/A_j*v_p;
    F_j = rho*A_j*v_j.^2;
    P_j = 1/2*rho*A_j*v_j.^3;

    %Generate outputs
    t = [0 t_vec t_max];
    v = [0 v_j 0];
    F = [0 F_j 0];
    P = [0 P_j 0];

    %Verify efficiencies
    E_out = trapz(t,P);
    Eff_sys_calc = E_out/E_in;
    Eff_sys_theo = Eff_fric*Eff_nozz;

end
```